Plastidial and cytosolic thiol reductases participate in the control of stomatal functioning

Jean-luc Montillet, Damien Rondet, Sabine Brugière, Patricia Henri, Dominique Rumeau, Jean-philippe Reichheld, Yohann Couté, Nathalie Leonhardt, Pascal Rey

Plastidial and cytosolic thiol reductases participate in the control of stomatal functioning

Journal:	*Plant, Cell & Environment*
Manuscript ID	Draft
Wiley - Manuscript type:	Original Article
Date Submitted by the Author:	n/a
Complete List of Authors:	Montillet, Jean-Luc; CEA, DRF, BIAM, PPV Rondet, Damien ; CEA, DRF, BIAM, PPV Brugiere, Sabine; CEA, DRF, IRIG, BGE Henri, Patricia; CEA, DRF, BIAM, PPV Rumeau, Dominique; CNRS7265, DRF, BIAM, PPV Reichheld , Jean-Phillipe; CNRS, LGDP Couté, Yohann; CEA, DRF, IRIG, BGE Leonhardt, Nathalie; CEA Cadarache, DRF, BIAM, SAVE Rey, Pascal; CEA, DRF, BIAM, PPV
Environment Keywords:	CO2, oxidative stress
Physiology Keywords:	signaling, stomata
Other Keywords:	redox signaling, thiol reductase
Abstract:	Stomatal movements via the control of gas exchanges condition plant growth in relation to environmental stimuli through a complex signaling network involving reactive oxygen species that lead to post-translational modifications of Cys and Met residues, and alter protein activity and/or conformation. Thiol-reductases (TRs), which include thioredoxins, glutaredoxins (GRXs) and peroxiredoxins (PRXs), participate in signaling pathways through the control of Cys redox status in client proteins. Their involvement in stomatal functioning remains poorly characterized. By performing a mass spectrometry-based proteomic analysis, we show that numerous thiol reductases, like PRXs, are highly abundant in guard cells. When investigating various Arabidopsis mutants impaired in the expression of TR genes, no change in stomatal density and index was noticed. In optimal growth conditions, a line deficient in cytosolic NADPH-thioredoxin reductases displayed higher stomatal conductance and lower leaf temperature evaluated by thermal infrared imaging. In contrast, lines deficient in plastidial 2-CysPRXs or type-II GRXs exhibited compared to WT reduced conductance and warmer leaves in optimal conditions, and enhanced stomatal closure in epidermal peels treated with abscisic acid or hydrogen peroxide. Altogether, these data strongly support the contribution of thiol redox switches within the signaling network regulating guard cell movements and stomatal functioning.

Plastidial and cytosolic thiol reductases participate in the control of stomatal functioning

Jean-Luc Montillet[1], Damien Rondet[1, 2], Sabine Brugière[3], Patricia Henri[1], Dominique Rumeau[1], Jean-Philippe Reichheld [4], Yohann Couté[3], Nathalie Leonhardt[5], Pascal Rey[1, *]

[1]Aix Marseille Univ, CEA, CNRS, BIAM, Plant Protective Proteins Team, F-13108, Saint Paul-Lez-Durance, France

[2]Laboratoire Nixe, F-06905 Sophia-Antipolis, France

[3]Univ. Grenoble Alpes, CEA, INSERM, IRIG, BGE, Grenoble, France

[4]Laboratoire Génome et Développement des Plantes, CNRS, Université Perpignan Via Domitia, F-66860 Perpignan, France

[5]Aix Marseille Univ, CEA, CNRS, BIAM, SAVE Team, Saint Paul-Lez-Durance, France F-13108

* Corresponding author: Pascal Rey; pascal.rey@cea.fr

Abstract

Stomatal movements *via* the control of gas exchanges condition plant growth in relation to environmental stimuli through a complex signaling network involving reactive oxygen species that lead to post-translational modifications of Cys and Met residues, and alter protein activity and/or conformation. Thiol-reductases (TRs), which include thioredoxins, glutaredoxins (GRXs) and peroxiredoxins (PRXs), participate in signaling pathways through the control of Cys redox status in client proteins. Their involvement in stomatal functioning remains poorly characterized. By performing a mass spectrometry-based proteomic analysis, we show that numerous thiol reductases, like PRXs, are highly abundant in guard cells. When investigating various Arabidopsis mutants impaired in the expression of *TR* genes, no change in stomatal density and index was noticed. In optimal growth conditions, a line deficient in cytosolic NADPH-thioredoxin reductases displayed higher stomatal conductance and lower leaf temperature evaluated by thermal infrared imaging. In contrast, lines deficient in plastidial 2-CysPRXs or type-II GRXs exhibited compared to WT reduced conductance and warmer leaves in optimal conditions, and enhanced stomatal closure in epidermal peels treated with abscisic acid or hydrogen peroxide. Altogether, these data strongly support the contribution of thiol redox switches within the signaling network regulating guard cell movements and stomatal functioning.

Summary statement: The contribution of thiol reductases to the signaling network governing stomatal functioning remains poorly known. Using proteomics, we show that numerous thiol reductases are abundant in a guard cell-enriched fraction, and we unveil a stomatal phenotype in Arabidopsis mutants for thiol reductases.

Keywords: *Arabidopsis thaliana*, glutaredoxin, guard cell, peroxiredoxin, proteomics, thiol reductase, signaling, stomata, thioredoxin.

Introduction

The movements of stomata, pores delimited by two guard cells, govern gas exchange and transpiration at the leaf surface. Plant growth is thus conditioned by stomatal opening, which allows CO_2 supply for photosynthetic assimilation, and ensures appropriate hydration and temperature in leaf tissues (Hetherington and Woodward, 2003; Berry et al, 2010). During stomatal movements, the turgor and volume of vacuole in guard cells change due to osmolyte fluxes thanks to the fine regulation of channels and carriers in plasma and vacuole membranes (Kim et al, 2010; Roux and Leonhardt, 2018). These movements result from the sensing of environmental stimuli (primary input signals), the production of secondary signals such as hormones and the signal transduction *via* numerous messengers including kinases, calcium ions and reactive oxygen species (ROS) (Murata et al, 2015; Kollist et al, 2014).

Stomatal opening is mainly caused by blue light and photosynthetic active radiations (Shimazaki et al., 2007; Kollist et al, 2014). In comparison, multiple primary stimuli promote stomatal closure to limit water loss in response to the varying environment that plants face (Kim et al, 2010; Murata et al, 2015). Abscisic acid (ABA) plays a central role in this process notably *via* the production of ROS, which are recognized signaling molecules in stomatal movements (Kwak et al, 2003; Song et al, 2014; Sierla et al, 2016). ROS fulfill signaling functions in development and responses to environment by reacting with antioxidant molecules, lipids and proteins (Foyer and Noctor, 2016). Oxidation of sulfur-containing amino acids, Cys and Met, leads to redox post-translational modifications and switches altering enzymatic activity, protein conformation or subcellular distribution (Delaunay et al, 2002; Tada et al, 2008; Geigenberger et al., 2017).

Plant thiol reductases (TRs), which display catalytic Cys, accomplish key biological functions including signaling by controlling Cys and Met redox status in partner proteins (Rouhier et al, 2015; Geigenberger et al, 2017; Rey and Tarrago, 2018). They belong to

multigene families (Tarrago et al, 2009; Meyer et al, 2012; Liebthal et al, 2018), and those considered here include thioredoxins (TRXs), glutaredoxins (GRXs), methionine sulfoxide reductases (MSRs) and the related thiol peroxidases: peroxiredoxins (PRXs) and glutathione peroxidases (GPXs) named by analogy to mammalian counterparts albeit using preferentially TRXs as reductants (Navrot et al, 2006). Plant TRXs are well-characterized small disulfide reductases carrying a Cys-Xxx-Xxx-Cys active site. Plastidial isoforms regulate photosynthetic metabolism in relation with light and redox pressure (Schürmann and Buchanan, 2008; Courteille et al, 2013; Naranjo et al, 2016). Cytosolic h-type TRXs are supplied in reducing power by NADPH-TRX reductases (NTRs), and participate in the mobilization of seed reserves upon germination or in responses to biotic constraints (Sweat and Wolpert, 2007; Hägglund et al, 2016). GRXs are oxidoreductases closely related to TRXs using glutathione (GSH) as an electron donor (Rouhier et al, 2008). Among TRX and GRX targets, thiol peroxidases play essential signaling roles *via* the control of peroxide concentration or direct thiol oxidation in protein partners (Day et al., 2012; Rhee and Woo, 2011; Stöcker at al., 2017). Thus, plastidial 2-CysPRXs participate in photosynthesis deactivation during the light-dark transition (Yoshida et al., 2018). Their signaling function is further supported by their ability to interact with more than 150 proteins (Cerveau et al, 2016a). Plant TRXs and GRXs, by modifying the Cys redox status in a very broad set of proteins (Rouhier et al, 2005; Montrichard et al, 2009), are involved in multiple metabolic, developmental and stress-related processes (Rey et al., 2005; Vieira Dos Santos and Rey, 2006; Bashandy et al., 2010: Knuesting et al, 2015; Rouhier et al, 2015; Liebthal et al, 2018). However, their involvement in stomatal functioning remains elusive. In a pioneer work, Jahan et al. (2008) reported enhanced ABA-induced stomatal closure in Arabidopsis GSH-deficient plants. Proteomic analyses showed high abundance of several TRs in Arabidopsis and *B. napus* guard cells (Zhao et al., 2008; Zhu et al., 2009; 2010), and identified potential TR partners in these cells (Zhu et al., 2014; Zhang et al., 2016). Of note,

GPX3 based on the phenotype of Arabidopsis mutants and on its ability to interact with ABA-related signaling actors was presumed to act as both a ROS scavenger and a redox transducer in guard cells (Miao et al, 2006). Changes in stomatal functioning have been also reported in plants modified for the abundance of plastidial 2-CysPRXs (Mao et al., 2018), mitochondrial TRXs o1 and h2 (Calderon et al., 2018; da Fonseca et al., 2019), or cytosolic GRXS17 (Hu et al., 2017).

Altogether, these data suggest that thiol redox switch, *via* the action of TRs, is a major component of the cell guard signaling network. However, the knowledge on this process is still very poor due to the limited data regarding the presence and abundance of TRs in guard cells. In this work, we characterized the proteome of a fraction highly enriched in guard cells and we present a detailed analysis of the expression of Arabidopsis *TR* genes. We found that numerous TRs are abundant in this fraction, and uncovered a stomatal phenotype for mutants deficient in NTRs, PRXs or GRXs. Finally, we discuss the potential functions of TRs in the signaling pathways governing stomatal movements.

Material and methods

Plant material

Arabidopsis plants were grown in the "Phytotec" platform (CEA, DRF, BIAM) from sowing in soil in standard conditions under an 8-h photoperiod and a photon flux density of 200 µmol photons.m^{-2}.s^{-1} with a temperature regime of 22/18°C (day/night) and a relative humidity of 55% as reported in Cerveau et al. (2016b). The genotypes used were wild-type Col-0, two T-DNA mutant lines for *TRXh3* (SAIL_314_G04 and SALK_111160), two T-DNA mutant lines for *TRXo1* (SALK_143294C and SALK_042792), one T-DNA mutant line for *PRXQ* (SAIL_742_G10), one T-DNA mutant line for *GRXS17* (SALK_021301), one double T-DNA mutant line for *2-CysPRXA* and *2-CysPRXB* (Cerveau et al., 2016b), one double T-DNA mutant

line for *NTRA* and *NTRB* (Reichheld et al., 2007), several lines either impaired for or over-expressing *GRXS14* and/or *GRXS16* (Rey et al., 2017), and the *ost2-2D* mutant (Merlot et al., 2007). Arabidopsis leaf genomic DNA from *trxh3* and *prxq* mutants was extracted using the Phire plant direct kit (Thermofisher) to perform PCR using appropriate primers corresponding to 5' and 3' ends of coding sequences, Taq DNA polymerase (Life Technologies), and the GeneAmp PCRSystem 2700 (Applied Biosystems). The absence of expression in homozygous plants was checked at the protein level. Rosette weight measurements were performed following 5 or 6 weeks of growth in standard conditions. Plants expressing promoter-GUS reporter constructs were previously described (Reichheld et al., 2002; Reichheld et al., 2007). GUS histochemical staining was performed according to Reichheld et al. (2007).

Preparation of fractions enriched in guard cells from leaf epidermis

Epidermis were prepared from six week-old plants grown in standard conditions. Leaves (35 g) were ground at max speed for 3 min in 1 L bowl of a Waring Blender™ containing about 200 ml deionised water and a handful of crushed ice. The suspension was filtered through 100-µm nylon sieve, and then rinsed off thoroughly with deionised water. The obtained retentate was rapidly dried on paper towels, suspended in 10 mM Tris-Mes buffer pH 6.0 containing 30 mM KCl 0.5 M NaCl and 0.5 mM SDS (1 g material in 5 mL buffer). The suspension was gently stirred at room temperature for 15 min before filtration (100 µm), rinsed with deionised water and dried on paper towels. After rapid freezing in liquid N_2, samples were stored at -20°C before protein extraction and analyses.

Protein extraction from leaf and epidermis fractions

Protein extracts, prepared according to Wang et al., (2006) from 0.5 g of leaf or epidermis, and sampled from three independent plant cultures were mixed to gain a representative sample

of each type of material. Protein concentration was determined using the "Protein Quantification BCA Assay" kit (Interchim). The resulting protein pellets were resuspended in sodium phosphate buffer 0.1 M pH 7.2 containing 0.15M NaCl and 1% SDS, diluted (1:4) in 4 X Laemmli buffer and heat-denatured 5 min at 95°C.

Mass spectrometry-based proteomic analyses

Twenty-five micrograms of proteins were stacked in a single band in the top of a SDS-PAGE gel (4-12% NuPAGE, Life Technologies) and stained with Coomassie blue R-250 before in-gel digestion using modified trypsin (Promega, sequencing grade) as previously described (Salvetti et al., 2016). Resulting peptides were fractionated by tip-based strong cation exchange and analysed by nanoliquid chromatography coupled to tandem mass spectrometry as previously described (Farhat et al. 2020).

RAW files were processed using MaxQuant (Tyanova et al., 2016) version 1.5.8.3. Spectra were searched against the Uniprot database (Arabidopsis thaliana reference proteome, February 2017 version), the frequently observed contaminants database embedded in MaxQuant, and the corresponding reversed databases. Trypsin was chosen as the enzyme and two missed cleavages were allowed. Precursor and fragment mass error tolerances were set at their default values. Peptide modifications allowed during the search were: Carbamidomethyl (C, fixed), Acetyl (Protein N-term, variable) and Oxidation (M, variable). Minimum number of peptides, razor + unique peptides and unique peptides were set to one. Maximum false discovery rates were set to 0.01 at PSM and protein levels. The match between runs option was activated. Quantification of proteins was based on unique + razor peptides. For sample comparison, intensity-based absolute quantification (iBAQ) values were loaded into ProStaR (Wieczorek et al., 2017). Peptides and proteins identified in the reverse and contaminant databases were discarded. After log2 transformation, iBAQ values were median normalized, and their log2(fold change)

between conditions calculated, after missing value imputation (replacing missing value by the mean first percentile of both samples).

Bioinformatics and data processing

Minimum number of peptides, razor + unique peptides and unique peptides were set to one. Maximum false discovery rates were set to 0.01 at PSM and protein levels. The match between runs option was activated. Quantification of proteins was based on unique + razor peptides. For comparison of samples, intensity-based absolute quantification (iBAQ) values were loaded into ProStaR (Wieczorek et al., 2017). Peptides and proteins identified in the reverse and contaminant databases were discarded. After log2 transformation, iBAQ values were median normalized and their log2 (fold change) between conditions calculated.

Electrophoresis and immunoblot analysis

Proteins were SDS-PAGE separated in reducing conditions, and either stained using Coomassie blue (Imperial™ Protein Stain, Thermo Scientific) or electroblotted onto 0.45 µm nitrocellulose (Pall Corporation) for immunoblot analysis. Primary antibodies raised against At2-CysPRX (Broin *et al.,* 2002), poplar PRXQ (Rouhier et al., 2004), AtPRXII-B (Bréhelin et al., 2003), AtTRX h3 (Reichheld et al., 2007) and AtGRXS14 (Rey et al., 2017) were used diluted 1:10,000, 1:1000, 1:10,000, 1:10,000 and 1:800, respectively. Antibodies against hyperoxidized 2-CysPRX (LF-PA0004; AbFrontier, Seoul, Korea) were diluted 1:3,000. The serum against spinach RubisCO (kindly provided by Dr. GH Schmid, University of Bielefeld, Germany) was diluted 1:10,000. Bound antibodies were detected using either a goat anti-rabbit secondary antibody coupled to a fluorescent molecule at a dilution of 1:10,000 (Alexa Fluor 680, Invitrogen) using the 'Odyssey Infrared Imager' at 680 nm (Licor, Lincoln, NE, USA) or an anti-rabbit immunoglobulin G coupled to alkaline phosphatase (Sigma).

204

205 **Chlorophyll content determination**

206 One-cm diameter leaf disks were taken from well-expanded adult leaves and crushed in
207 1 mL 80% acetone. Following vigorous shaking, overnight storage in the dark at 4°C and
208 centrifugation (14,000 g, 10 min), the chlorophyll content was measured
209 spectrophotometrically, and calculated according to Lichtenthaler (1987).

210

211 **Preparation of adaxial and abaxial leaf epidermis for stomatal counting.**

212 Adaxial (upper) and abaxial (lower) epidermis were prepared according to a protocol
213 derived from the "Tape-Arabidopsis Sandwich" reported by Wu et al., (2009). The upper or
214 lower epidermal surface was stuck on a strip of Time tape (Time Med, IL., USA) while the
215 opposite surface was affixed to a strip of Scotch Crystal tape (3M, Minn., USA). The Scotch
216 Crystal tape was then sharply removed, and put in a Petri dish containing 10 mM Tris-Mes
217 buffer pH 6.0, 30 mM KCl to avoid tissue desiccation. Then with the help of a microscope cover
218 slip, the strip has been scraped off to get rid, the best as possible, of mesophyll tissues. Stomata
219 were counted with the help of a Leica LMD6000 microscope. Stomatal index was calculated
220 using the formula S/(E + S), S being the number of stomata per area unit and E the number of
221 ordinary epidermal cells in the same area.

222

223 **Measurements of stomatal aperture**

224 The abaxial side of half leaf blades from two 4–5-week-old plants of the same genotype
225 grown in standard conditions was stuck on cover slips and peeled. Samples were then placed in
226 Petri dishes containing 20 mL of buffer containing 10 mM MES/Tris pH 6.0, 30 mM KCl. After
227 30 min in the dark, epidermal peels (except controls) were transferred under light (300 µmol
228 photons.m^{-2}.s^{-1}) at 22°C for 2.5 h in order to ensure that most stomata were open before

treatments. For promotion of closure, 20 µL of stock solutions of ABA in ethanol and of H_2O_2 in water were directly diluted in the buffer in contact with peels. Thereafter, samples were incubated in the light for 2.5 h before aperture measurements according to Merlot et al., (2007). To avoid bias results, double blind experiments were performed, so that, experimenters in charge of measurements were not informed of genotype or treatment. Values reported are the means ± SD of two independent experiments, for which 60 aperture widths were measured each time. Error bars represent standard deviations of the means.

Porometry measurements

Stomatal conductance of fully expanded leaves was measured on 6-week old well drained plants grown in standard conditions. Measurements were carried out using a hand-held AP4 porometer (Delta-T Devices, Cambridge, UK) on the abaxial leaf side in the middle of the light period, and two to four hours after watering by flooding. Usually, eight measurements per plant were made on 6 to 12 independent plants per genotype. Due to variations in calibration resulting from slight differences in the moisture of the paper used as a reference, differences were noticed in the level of conductance in WT plants between experiments despite very similar growth and measurement conditions. All experiments and repetitions for characterizing one genotype and corresponding WT plants were carried out using the same calibration reference.

Infrared determination of leaf temperature

Plants were cultivated on soil as described above for up to 6 weeks in a dedicated phytotron, in which low relative humidity (45% ± 5%) and low wind speed were applied the day before infrared thermographic imaging to ensure optimal contrast between lines. Images were acquired using a Thermacam PM250 infrared camera as described by Costa et al., (2015).

Results

Analysis of *TR* gene expression in guard cells by transcriptomics

As a first step, using transcriptomic data from guard and mesophyll cell protoplasts representing a large part of Arabidopsis genes (Yang et al., 2008), we extracted those available for *TR* genes. Based on relative expression values, we noticed that most TR transcripts are present in both cell types (data not shown), and observed that a number of them displayed a ratio between the two values higher than 2, indicating preferential expression in one cell type. This was noticed for *NADPH-Thioredoxin Reductase A* (*NTRA*), which encodes the reducer for cytosolic TRXs and exhibits higher transcript level in guard cells (Fig. S1A). Regarding *TRX* genes (Fig. S1A), we observed that *TRXh3* exhibits compared to others the highest expression in guard cells, and a substantially higher transcript level compared to mesophyll cells. Most interestingly, nine other *TRX* genes (*h2*, *h4*, *m3*, *o1*, *o2*, *TDX*, *CLOT*, *NRX1* and *LILIUM-1*), coding for various typical or unusual isoforms located in the main subcellular compartments, exhibited higher expression in guard cells, while two (*h5* and *CDSP32*) were preferentially expressed in mesophyll cells. Regarding other *TR* genes (Fig. S1B), we noticed that *GRXs S15* and *ROXY10, PRXII-B* and *GPX2*, and *MSRs A1* and *A4* displayed a transcript abundance higher in guard cells compared to mesophyll cells. To deepen some of these microarray data, we analyzed gene expression by promoter-GUS histochemistry (Fig S2). GUS staining was clearly observed in guard cells of *PrTRXh2-*, *PrTRXh3-*, *PrPRXII-B-* and *PrNTRB-GUS* lines, confirming the expression of these *TR* genes in guard cells.

Preparation of a guard cell-enriched fraction

We then investigated *TR* gene expression in guard cells by implementing a proteomic approach. We did not used protoplasts since during preparation, redox homeostasis is dramatically impaired (Papadakis and Roubelakis-Angelakis, 1999), leading to changes in the

expression, abundance, redox status and conformation of TRs. To obtain a fraction enriched in guard cells, we treated epidermis from Arabidopsis plants as described in Experimental Procedures. Microscope observations of this fraction revealed the presence of intact guard cells, predominantly broken and open pavement and trichome cells, and some pieces of xylem vessels (data not shown). The presence of chloroplasts served as an indication of cell integrity. Vigorous shearing of leaf tissues and extensive washing of epidermis kept intact only guard cells, which are protected from mechanical constraints due to their cell wall thickness. We therefore assumed that a significant part of proteins in this extract, notably the soluble pool, originates from guard cells. To estimate the enrichment, we counted guard cells in both epidermal sides of all leaves of 6-week old plants, measured the sizes of representative guard cells to estimate their average volume, and determined the protein concentrations in whole leaves and in broken epidermis. Based on these measurements (Table S1), the total GC volume has been rated at 0.13% of the leaf volume, and assuming that protein concentration (2 $mg.g^{-1}$ leaf FW) is identical regardless of cell type, we estimated this content in GC to 0.0026 $mg.g^{-1}$. Given that the protein concentration in grinded epidermis was 0.028 $mg.g^{-1}$ FW, the inference is that 9.3 % come from guard cells. Therefore, we calculated an enrichment factor of 71 (9.3:0.13) in broken epidermis that was thus termed guard cell-enriched (GCE) fraction. Finally, we compared the protein patterns of leaf and GCE fractions by SDS-PAGE (Fig. 1A), and observed clear differences, such as dramatically decreased abundance of RubisCO subunits at 50 and 13 kDa in the GCE fraction. This was confirmed in immunoblots, where a much higher band intensity was observed for both subunits in the leaf extract (Fig. 1B). In contrast, the intensity of two bands at 22 and 75 kDa was more elevated in the GCE fraction (Fig. 1A).

Proteomic analysis of the GCE fraction and extracted abundance of guard cell actors

The GCE fraction, along with a whole leaf extract prepared in a similar manner, were analyzed by mass spectrometry-based proteomics, leading to the characterization of 4842 proteins identified with two peptides and quantified in at least in one of the two samples, representing 4694 and 4248 proteins in GCE and leaf fractions, respectively (Table S2). To estimate the relative abundance in each sample, we ranked proteins according to their computed intensity-based absolute quantification (iBAQ, Schwanhäusser et al., 2011) values. The iBAQ values were also used to compare the abundance of each protein between GCE and leaf fractions. The functional categorization of the genes encoding the 25 % most abundant proteins in each fraction has been determined using the Gene Ontology annotation retrieval tool available on the TAIR site (https://www.arabidopsis.org/tools/go_term_enrichment.jsp). The comparison uncovered some striking differences (Fig. 2), such as under-representation (- 9 to -16%) of proteins related to plastid, chloroplast and thylakoid functioning in the GCE fraction, consistent with the elimination of photosynthetic mesophyll cells during the preparation.

We also noticed enrichment (+ 9%) in the GCE fraction of extracellular and cell wall proteins (Fig. 2), partly due to the presence of many cell phantoms originating from the pavement. With the help of the reports of Irshad et al., (2008), Duruflé et al., (2019) and Showalter et al., (2010) that characterized Arabidopsis cell wall proteome using bioinformatic and proteomic approaches, we reckoned 322 proteins contributing to cell wall structure or function (Table S3). A majority (85%) is more abundant in the GCE fraction, 16% being not detected in leaf. Of note, based on microarray data (Yang et al., 2008), more than one third of the genes encoding these proteins were found preferentially expressed in GC (ratio of expression GC/MC higher than 2). Regarding extracellular proteins (Table S3), seven germins and germin-like proteins (GLPs) are more abundant in the GCE fraction, two (GLP1-6 and GLP5-1) being the first and the fifth most abundant proteins, respectively. GLPS are

329 glycoproteins associated with the extracellular matrix, encoded by 32 genes in Arabidopsis, and
330 involved in responses to osmotic constraints (Li et al., 2016). Among cell wall proteins more
331 abundant in the GCE fraction (Table S3), we noticed the presence of a large number of GDSL-
332 type esterases/lipases, 18 out of 45 putative ones, which are notably involved in biotic stress
333 responses (Lai et al., 2017), and of 17 expansins out of the 36 genes identified in Arabidopsis
334 (Lee et al., 2001). Expansins interact with cell wall carbohydrates, cellulose and hemicellulose.
335 Most interestingly, expansin A1, which plays a critical role in stomatal movements (Wei et al.,
336 2011; Zhang et al., 2011), is one of the most abundant protein (rank 29) in the GCE fraction.
337 In other respects, Leonhardt et al. (2004) identified 63 genes preferentially expressed in
338 guard cells, 25 being present in our analysis. Table S4 shows that only one protein encoded by
339 this set of genes is more represented in the leaf fraction, and that 20 are more abundant in the
340 GCE fraction, eight being specific of this sample. Finally, to further figure out the validity of
341 the GCE fraction regarding stomatal functions, we scrutinized the protein list to find out
342 candidates previously described as key players in stomatal movements or development (Table
343 1). Hence, 56 of these proteins were pinpointed, 43 being more abundant (R value > 1.5) in the
344 GCE fraction than in leaf. Consistently, a large majority of genes encoding these proteins are
345 more expressed in guard cells than in mesophyll cells (Table S4) (Yang et al., 2008), and 22
346 were identified in Arabidopsis GC protoplasts (Zhao et al., 2008, 2010). Among the 56 proteins,
347 we identified 12 kinases and phosphatases, 14 ion channels, pumps and transporters, 3 ABA
348 receptors, and 19 enzymes and other proteins acting in osmoregulation in guard cells, in
349 addition to eight effectors involved in stomatal development and patterning. We also identified
350 GRF6 (14-3-3 λ) that is involved in blue light-mediated stomatal opening (Tseng et al., 2012),
351 and present in the GCE fraction at a high level (top 5%). 14-3-3 proteins (GRFs) are regulators
352 of stomatal movements (Cotelle and Leonhardt, 2016), through the binding of phosphorylated
353 client proteins such as phototropins, plasma membrane H^+-ATPases or ion channels. In our

analysis, we detected 10 out of the 13 members of this family, all being more abundant in the GCE fraction (Table S5). Taken together, these data indicate that grinding and extensively washing epidermis is as an easy way to concentrate guard cell proteins as evidenced by the high enrichment factor and the exclusive presence in the GCE fraction of numerous proteins known to function in stomatal movements. This approach can be thus used for identifying new proteins, the activity of which could be determinant for guard cell functioning.

Abundance of TRs in the GCE fraction

We thus analyzed the protein list from the GCE fraction to retrieve all TRs, and ranked them according to extracted abundance (Table 2). Thirty-nine TRs, out of the approximately 100 genes belonging to these enzyme families in *Arabidopsis thaliana*, were identified. Most interestingly, we observed the presence of various PRXs (PRXQ, 2-CysPRXA, PRXII-B, PRXII-F) in the first decile, and of other TR types (NTRA, PRXII-E, TRX h3, GPX6, 2-CysPRXB, MSRA2, NRX1) in the first quartile. Numerous TRs (NTRB, MSRA4, GPX1, GPX2, TRX z, TRX h2, TRX m2, NTRC, TRX f1) were present in the first half of the ranking list. Then, we compared the relative abundance of TRs in GCE and leaf fractions using the R parameter (Table 2). When selecting those displaying a R value superior to 1.5, we pointed 19 TRs, many being much more abundant in the GCE fraction than in leaf, notably PRXII-B, NTRA, TRX h3, MSRA2, NRX1, NTRB, GPX2, TRX h2, GPX3 and TRX CxxS1. Of note, five TRs were only detected in the GCE fraction, namely TRX z, TRXh9, GRXS15, TDX and TRX Lilium 6. In other respects, we also searched for the TRs relatively more abundant in the leaf fraction. We found that all those having a very low R value (< 0.1) are involved in the regulation of photosynthesis or in the maintenance of plastidial redox homeostasis. This is the case of TRXs m1, m2, m4, f1, CDSP32, HCF164, and MSRB2. By crossing transcriptomic and proteomic data (Fig. S1, Table 2), we observed good consistency between the two approaches.

Indeed, among the 17 *TR* genes displaying preferential expression in GC, 11 were identified by proteomics and nine encode proteins more abundant in the GCE fraction. Finally, by comparing with the pioneer proteomic works on guard cell protoplasts, in which a much lower number of proteins (*ca* 1000) was identified, we noticed that all TRs detected in these reports (Zhao et al., 2008; 2010) are present in the GCE fraction (Table 2). Altogether, these findings lead us to conclude that numerous TRs are present in guard cells, several of them being very abundant.

Western blot analysis of TR abundance in the GCE fraction

We then assessed the abundance of some TRs in the GCE and leaf fractions by Western blot analysis (Fig. 1B). We noticed a much higher amount of TRX h3 in the GCE fraction than in leaf, and observed relative abundances of 2-CysPRXs, PRXQ, PRX-IIE and PRXII-B in the two fractions consistent with proteomic data. Further, we noticed comparable abundance in the two fractions of GRXS14, which was not detected in the proteomic analysis. Most interestingly, substantial changes in the redox status of 2-CysPRXs and GRXS14 were detected in the GCE fraction. Indeed, while the level of hyperoxidized 2-CysPRXs was relatively low in leaf, as already observed (Cerveau et al. 2016b; Cerveau et al. 2019), this form was much more abundant in the GCE fraction. Regarding GRXS14, we previously reported that the GRX has two redox forms showing differential migration (Rey et al., 2017). Whereas only one redox GRXS14 form was detected in leaf proteins, two specific bands were revealed in the GCE fraction. These data reveal that TRs could display specific redox features in guard cells compared to photosynthetic cells.

Phenotype of mutants impaired in the expression of *TR* genes

To gain further insights about TR functions in stomatal biology, we investigated the phenotype of mutants modified for the expression of *PRXQ*, *2-CysPRXs*, *NTRA and NTRB*,

404 *TRXh3*, *TRXo1*, *GRXS17*, *GRXS14* or *GRXS16*. These lines were selected based on protein
405 abundance in guard cells, mutant availability (Reichheld et al., 2007; Knuesting et al., 2015;
406 Cerveau et al., 2016b; Rey et al., 2017; Calderon et al., 2018), bibliographical data (Hu et al,
407 2017; Calderon et al, 2018; Mao et al, 2018), and preliminary experiments. Regarding *prxq* and
408 *trxh3* mutants, gene disruption was validated at the protein level (Fig. S3).

409 First, we investigated the growth of mutants in standard short-day, light, temperature and
410 watering conditions, in which stomata function in an optimal manner. Growth was characterized
411 by measuring the rosette fresh weight of 5- to 6-week old plants (Fig. S4). We previously
412 reported that Arabidopsis plants impaired for both *GRXS14* and *GRXS16* expression displayed
413 reduced growth (Fig. S5), whereas those over-expressing *GRXS14* exhibited higher rosette
414 weight (Rey et al., 2017). Plants deficient in *GRXS17* expression did not exhibit any growth
415 phenotype in short photoperiod (Fig. S4C) as already observed (Knuesting et al., 2015).
416 Regarding lines affected in plastidial PRXs, we did not observe any difference for *prxq* as
417 reported for another mutant (Lamkemeyer et al. 2006), but noticed that 2-*cysprxa* 2-*cysprxb*
418 plants displayed substantially reduced growth (Figs. S4A, S5), consistently with the reports of
419 Pulido et al., (2010) and Awad et al., (2015). A somewhat reduced growth was noticed for *ntra*
420 *ntrb* plants (Figs. S4B, S5) as in Reichheld et al., (2007), and *trxh3* and *trxo1* plants displayed
421 slightly higher, but non-significantly different, rosette weights in agreement with Park et al.
422 (2009) on one *trxh3* line, and Ortiz-Espin et al. (2017) on two *trxo1* mutants (Fig. S4D-E).

423 In addition, we measured the chlorophyll content and observed that most lines displayed a
424 level similar to that in WT (Fig. S6), except the 2-*cysprxa* 2-*cysprxb* mutant, which exhibited
425 pale green leaf phenotype (Fig. S5) and chlorophyll content reduced by *ca* 20% (Fig. S6) as
426 observed by Pulido et al., (2010). In other respects, the two lines over-expressing *GRXS14* were
427 previously reported to display a somewhat reduced pigment content (Rey et al., 2017).
428

Stomatal phenotype of mutants impaired in the cytosolic NTR/TRX system

We then characterized TR-modified lines with regard to stomatal functioning, and first investigated the phenotype of those deficient in cytosolic NADPH-thioredoxin reductases A and B, TRXs h3 or o1. Beforehand, we determined the density and number of stomata in relation with the number of epidermal cells (stomatal index), since variations in these parameters can lead to differences in leaf capacity for gas exchange. We observed very close values of density (ca 270 per mm^2) and index (0.16) in WT, *ntra ntrb* plants, *trxh3* and *trxo1* mutants (Fig. 3A-B; Fig S7A-B), indicating no change in stomatal differentiation and development in the absence of cytosolic NTRs, TRXs h3 or o1.

Porometry measurements were conducted to evaluate the stomatal conductance by measuring the rate of water efflux from the leaf abaxial side of plants grown in optimal conditions. We observed that the mutant lacking both cytosolic NTRA and NTRB displayed a significantly higher conductance compared to WT (182.4 ± 10.5 mmoles $H_2O.m^{-2}.s^{-1}$ *vs* 162.7 ± 16.9) (Fig. 3C). No variation in stomatal conductance was detected in *trxh3* and *trx o1* plants (Fig S8A-C). We then approached the stomatal functioning in 6-week old plants cultivated in standard conditions by evaluating leaf temperature using infrared (IR) imaging, since leaf cooling is ensured by opening of stomata. To validate the approach, we used the *ost2-2D* (*open stomata 2*) dominant mutant that displays stomatal closure defects due to constitutive H^+-ATPase activity (Merlot et al., 2007). IR imaging revealed a strong difference in the leaf temperature of this mutant compared to WT. In the *ost2-2D* mutant, most leaves appear purple/blue corresponding to a temperature in the range of 16 to 16.5°C, whereas in the WT the leaf color (green to yellow) reflected a temperature in the range of 17.2 to 17.8°C (Fig. 3D). This is consistent with constitutive wide stomatal opening and constant cooling in *ost2-2D* plants. Regarding mutants lacking either TRX h3 or TRX o1, no difference in leaf temperature was observed (data not shown). When examining *ntra ntrb* plants, we observed that their

454 temperature was lower than that of WT, as evidenced by the much higher number of red to
455 yellow leaves in the latter (Fig. 3E). Based on the color scale, the difference could be evaluated
456 to *ca* 0.5°C. Taken collectively, these data reveal that cytosolic NTRs that are highly abundant
457 in the GCE fraction (Table 2) participate in stomatal functioning.
458
459 **Stomatal phenotype of lines deficient in plastidial PRXs**
460 As previously shown (Table 2), plastidial PRXs are well represented in the GCE fraction,
461 PRXQ being the most abundant TR and 2-CysPRXA and B present in the top-ten proteins. We
462 thus investigated the phenotype of lines lacking these PRXs. Compared to WT, no difference
463 was observed in either stomatal density or index in both *2cysprxa 2cysprxb* and *prxq* plants
464 (Fig. 4A-B). In standard watering conditions, a significantly lower stomatal conductance was
465 measured in those deficient in 2-Cys-PRXs (*ca* 220 mmoles $H_2O.m^{-2}.s^{-1}$ *vs* 260 in WT), while
466 a slight non-significant decrease was noticed in *prxq* plants (Fig. 4C). When using thermal
467 infrared imaging, we noticed that many leaves of the mutant lacking both 2-CysPRXs displayed
468 red to yellow color corresponding to a temperature between 17 and 18°C, whereas most WT
469 leaves were green to red with a temperature between 16.5 and 17.5°C (Fig. 4D). With regard to
470 *prxq* plants, we noticed no substantial temperature difference compared to WT (Fig. 4E).
471
472 **Stomatal phenotype of lines deficient in type-II GRXs**
473 We then investigated the phenotype of Arabidopsis lines affected in the expression of type-
474 II GRXs based on the presence of cytosolic GRXS17 and plastidial GRXS16 in the GCE
475 fraction (Table 2), and on the report of Hu et al. (2017) showing a stomatal phenotype in
476 *GRXS17*-silenced rice plants. The Arabidopsis line deficient in GRXS17 did not exhibit any
477 variation in stomatal density and index (Fig. S7A-B) in short-day conditions, in which the

mutant has no obvious phenotype (Knuesting et al., 2015). No noticeable change in either stomatal conductance (Fig. S8D) or leaf temperature (data not shown) was observed.

We performed the analysis of lines modified for the expression of the two genes encoding plastidial type-II GRXs, GRXS14 and GRXS16 (Rey et al., 2017). First, we examined knockout mutants for *GRXS14*, lines co-suppressed for *GRXS16* (Rey et al., 2017), and lines overexpressing one of the two GRXs. No change was observed in the density and stomatal index of any of these lines (Fig. 5A-B: Fig. S7C-D), nor in the stomatal conductance (Fig. 5C; Fig. S8E-G) and leaf temperature (Fig. 5D, data not shown).

Finally, we analyzed the phenotype in standard growth conditions of two independent lines, termed KI1 and KI2, knockout for *GRXS14* and impaired for *GRXS16* expression due to RNA-interference (Rey et al., 2017). Compared to WT, both lines did not exhibit any significant variation in stomatal density and index (Fig. 5A-B). Interestingly, substantially reduced stomatal conductance was recorded in the two KI1 and KI2 lines compared to WT (*ca* 230 and 240 mmoles $H_2O.m^{-2}.s^{-1}$, respectively, *vs* 280 in WT) (Fig. 5C). Consistently, when imaging leaf temperature, we observed higher temperature in both lines (Fig. 5D-E). This was particularly obvious in the KI1 line, where all leaves, particularly the youngest ones, displayed a red to yellow color corresponding to a temperature in the range of or higher than 18°C, whereas most WT leaves exhibited green to red color with a temperature lower than 17.5°C.

Stomatal responses to ABA and H_2O_2 in lines deficient in thiol reductases

Considering that ABA and H_2O_2 are major actors promoting stomatal closure, we investigated whether mutants deficient in thiol reductases showed altered sensitivity to these compounds. Stomatal apertures were measured in light-pretreated epidermal peels, incubated for 2.5 h on buffer containing 0.5 to 100 µM ABA or 0.01 to 1 mM H_2O_2 (Fig. 6). We observed that at the lowest ABA concentration (0.5 µM), *2cysprxa 2cysprxb*, KI1 and KI2 plants were

much more reactive compared to WT and *ntra ntrb* plants. Indeed, whereas the latter displayed no change compared to light treatment alone, stomatal aperture was significantly decreased by *ca* 24% in *2cysprxa 2cysprxb*, KI1 and KI2 (Fig. 6A-B). At 1 µM, this differential behavior tended to diminish since a significant difference was observed only between WT and *2cysprxa 2cysprxb*, with aperture decreases of 20 and 40%, respectively. No difference among all lines was noticed at higher hormone concentrations. When epidermal peels were exposed to H_2O_2, substantial differences were observed for *2cysprxa 2cysprxb*, KI1 and KI2 lines, which clearly displayed enhanced sensitivity. In the three lines, stomatal aperture at 10 µM H_2O_2 was reduced by *ca* 35% and significantly lower compared to that recorded in WT and *ntra ntrb* plants (-10%) (Fig. 6 C-D). Higher susceptibility was also recorded at 100 µM H_2O_2 for the three mutant lines, but not at the highest concentration (1 mM). Altogether, these data indicate that plastidial thiol reductases modulate ABA- and H_2O_2-dependent signaling pathways controlling stomatal closure.

Discussion

Presence and abundance of TRs in guard cells

So far, the knowledge about the abundance of TRs in guard cells is limited and based on the proteome of guard cell protoplasts in *Arabidopsis thaliana* and *Brassica napus* (Zhao et al., 2008; 2010; Zhu et al, 2009; 2010). We attempted to strengthen this knowledge by taking advantage of the great advance in mass spectrometry-based proteomics made since. To avoid redox biases and changes due to protoplast preparation, we implemented another approach using broken and extensively washed epidermis to get a fraction highly enriched in guard cells. The enrichment of this fraction was validated by the relatively high abundance of numerous key actors involved in stomatal functioning (Table 1). With regard to TRs, the proteomic analysis of the GCE fraction highlighted several findings: i) among about 4700 proteins

identified, 39 TRs belonging to the TRX, GRX, PRX, GPX and MSR families are present; ii) *ca* half of them are relatively more abundant in the GCE fraction than in leaf. iii) NADPH-thioredoxin reductases A and B, the electron source for extra-plastidial TRXs, are present in the first quartile when ranking proteins as a function of abundance within the GCE fraction (Table 2); iv) six PRXs (PRXQ the most abundant TR, the two 2-CysPRXs and three PRX-IIs: B, E and F) out of the nine in Arabidopsis are also present in the first quartile of the list. Most importantly, these proteomic data are in accordance with transcriptomics of guard cell protoplasts, that revealed higher transcript levels for various TR types compared to mesophyll cells (Fig. S1). Further, all the TRs (13) identified in the first proteomic analyses of guard cell protoplasts in *Arabidopsis thaliana* and *Brassica napus* (Zhao et al., 2008; 2010; Zhu et al., 2009) are present in the GCE fraction, notably four PRXs (2-CysPRXA and B, PRXII-E and PRXII-F). Thereby, these reports and the present work strongly support a key contribution of TRs in the functioning of guard cells. Numerous TRs are present in both GCE and leaf fractions (Table S2), indicating that they might also participate in long-distance signaling pathways originating from mesophyll and controlling stomatal movements in relation with photosynthesis level (Lawson, 2009). Nonetheless, our data revealing high abundance of many TRs in guard cells and phenotypes for mutants impaired for several of them, give strong reliability to essential roles of these reductases within the stomatal signaling network and machinery.

Participation of cytosolic TRs in stomatal functioning

We observed that plants deficient in NTRA and NTRB display increased stomatal opening in standard growth conditions as evidenced by porometry measurements and thermal infrared imaging (Fig. 3). In other respects, bioassay experiments carried out on epidermal peels did not reveal any substantial aperture change in this line compared to WT in response to ABA or H_2O_2 treatments applied over a relatively short period of time (2.5 h) (Fig. 6). Both NTRs ensure the

553 reduction of cytosolic and mitochondrial TRXs, such as h and o isoforms. Nonetheless,
554 Arabidopsis mutant plants lacking either cytosolic TRX h3 or mitochondrial TRX o1 did not
555 show any noticeable change in stomatal functioning (Fig. S8). Interestingly, da Fonseca-Pereira
556 et al., (2019) reported that *ntra ntrb* and *trxo1* plants displayed faster recovery after two cycles
557 of drought episodes in relation with higher stomatal conductance. This is consistent with our
558 data unveiling higher conductance in the mutant lacking cytosolic and mitochondrial NTR
559 systems. Therefore, the role of the NTR/TRX system in stomata might be of importance
560 following drought stress. In other respects, Calderon et al. (2018) reported higher stomatal
561 density and index in the two *trxo1* mutant lines compared to WT, revealing a possible role of
562 these TRXs in stomatal development. When characterizing these mutants, we did not notice
563 such a phenotype. (Fig. S7). It is worth mentioning that in this study, the density and index
564 ranges (*ca* 120.mm^{-2} and 0.45) are very different from ours. This might originate from different
565 culture conditions and measurements performed at distinct developmental stages in the two
566 works. Of note, the *trxo1* lines also displayed reduced water loss upon high salinity, possibly
567 due to altered stomatal functioning (Calderon et al., 2018). Finally, da Fonseca-Pereira et al.,
568 (2020) reported that Arabidopsis mutants lacking TRX h2, which is located in both cytosol and
569 mitochondria, do not exhibit any growth phenotype in short day and low light intensity, but
570 decreased stomatal conductance and higher water use efficiency. These data indicate that the
571 cytosolic NTR/TRX system could fine tune guard cell functioning in relation with light
572 parameters via pathways remaining to be unveiled (Fig. 7).

573 This system is likely to fulfill several functions through redox interaction with known
574 actors of the signaling network regulating stomatal movements. Thus, cytosolic TRs might
575 control the redox status of OST1/SnRK2.6, BAK1, SnRK2.4 and CPK21, which are likely
576 prone to thiol-based modifications as they display cysteine thiol redox switches modifying their
577 activity *in vitro*, or interact *in vitro* with TRs (Bender et al. 2015; Wang et al. 2015; Zhu et al.

2017; Ma et al. 2018). This hypothesis is further supported by the identification of *ca* 80 potential TRX targets in a fraction enriched in guard cells (Zhang et al., 2016), and of numerous proteins harboring redox sensitive Cys in *Brassica napus* guard cells (Zhu et al., 2014). One major challenge will consist of identifying their reductants among TRs and determining their physiological functions in stomatal movements (Fig. 7).

Participation of plastidial TRs in stomatal functioning

Plants deficient in type-II GRXs or 2-Cys PRXs exhibited decreased stomatal opening in optimal growth conditions as shown by porometry and thermal infrared imaging (Figs. 4-5), and enhanced stomatal closure in epidermal peels treated with ABA or H_2O_2 (Fig. 6). H_2O_2 is an essential redox signaling messenger promoting closure, and likely enters the cytoplasm of guard cells (Rodrigues et al., 2017) following the ABA-induced ROS burst in apoplast (Kwak et al., 2003). Our data clearly reveal that GRXS14, GRXS16 and 2-CysPRXs limit ABA- and ROS-induced stomatal closure (Fig. 6). Strikingly, these reductases are located in plastids, highlighting the involvement of this compartment in stomatal functioning. This is fully consistent with the hypothesis of redox signals originating from chloroplasts in the network controlling stomatal movements (Chen and Gallie, 2004; Song et al, 2014), H_2O_2 accumulation in chloroplasts of guard cells being even considered as one of the earliest hallmarks of stomatal closure (Sierla et al, 2016). The involvement of subcellular compartments is further supported by the participation of mitochondrial TRX o1 in guard cell functioning (Calderon et al., 2018), and the presence of numerous organelle TRs in the GCE fraction (Table 2). Plastidial and mitochondrial TRs play master roles in energy generation and consumption (Schurmann and Buchanan, 2008; Daloso et al., 2015), and are thus probably needed in the regulation and coordination of the highly active metabolism in guard cells during stomatal movements.

Plastidial GRXS14 and S16 might modulate stomatal movements *via* the control of Cys redox status in partner proteins that participate in ROS-related transduction pathways inducing closure (Fig. 7). Consistent with this hypothesis, another GRX is able to inhibit *in vitro* the activity of BAK1 *via* glutathionylation (Bender et al., 2015). So far, very little is known *in vivo* about the participation of GRXs in stomatal functioning, except for GRXS17, which also belongs to class-II and is located in cytosol and nucleus. Silencing of its expression in rice is associated with increased stomatal closure (Hu et al., 2017). Moreover, GRXS17-deficent lines are more tolerant to water deficit (Hu et al., 2017). However, when investigating the stomatal phenotype of an Arabidopsis *grxs17* line using porometry and thermal imaging, we did not notice any difference with WT in standard conditions (Fig. S8 and data not shown), indicating environmental and/or species influence on the role of the GRX.

The Arabidopsis line lacking plastidial 2-CysPRXs exhibited a marked stomatal phenotype (Figs. 4, 6), which might underlie, at least partially, its decreased growth (Fig. S4) due to reduced CO_2 supply to photosynthetic cells. It is worth mentioning that this pleiotropic mutant also displays less chlorophyll (Figs. S5-S6) and increased susceptibility to photooxidative stress (Awad et al., 2015). Note that deficiency and overexpression of 2-CysPRX in rice lead to enhanced and decreased stomatal opening, respectively (Mao et al., 2017), suggesting that this peroxidase plays distinct roles in stomata of monocotyledons and dicotyledons. 2-Cys PRXs are considered as a central redox buffer in plastid since they are efficient scavengers of hydrogen and organic peroxides (Liebthal et al., 2018; Cerveau et al., 2019). Thus, they are prime candidates to sense local changes in H_2O_2 content in guard cells. This function could take place in the transduction pathway involving H_2O_2 and promoting stomatal closure. Since H_2O_2-induced closure is strongly enhanced in the mutant lacking both 2-Cys PRXs (Fig. 6), we can hypothesize that these peroxidases directly mitigate, *via* scavenging, the peroxide signal intensity leading to closure (Fig. 7). Further, many recent lines of evidence revealed that these

enzymes achieve essential roles in redox signaling processes through the control of thiol switch in partner proteins (Rhee and Woo, 2011; Liebthal et al., 2018). Accordingly, Stöcker at al. (2017) reported that 2-CysPRXs enable rapid and sensitive thiol oxidation in various protein types at the expense of H_2O_2. In plants, 2-CysPRXs play a key role in Calvin cycle deactivation at night *via* oxidation of TRX partners (Yoshida et al., 2018). Further, 2-Cys PRXs interact with a large number of potentially redox-regulated proteins (Cerveau et al., 2016a; Liebthal et al., 2020). Some such as β-amylases, which are redox-regulated enzymes involved in starch degradation, very likely participate in osmotic adjustment during stomata opening (Valerio et al., 2011; Horrer et al., 2016). Thus, we can presume that similarly to their role in photosynthesis regulation, 2-Cys PRXs participate in the daytime control of starch degradation, which drives light-induced stomatal opening (Horrer et al., 2016). Such a function might underlie the phenotype observed in whole plants (Fig. 4). To conclude, plastidial 2-Cys PRXs are likely to accomplish several signaling functions in relation with H_2O_2 level in guard cells (Fig. 7). This hypothesis is further supported by the much higher level of protein hyperoxidation in the GCE fraction compared to leaf (Fig. 1B). Cys hyperoxidation to a sulfinic acid form is reversible thanks to the action of sulfiredoxin (Rey et al., 2007), and leads based on the floodgate theory to local H_2O_2 accumulation and initiation of signaling pathways (Poole et al., 2011). Finally, 2-CysPRXs possess several phosphorylation sites (Liebthal et al., 2018) susceptible to modulate peroxidase activity as shown in its human counterpart (Woo et al., 2010) and possibly underlying interplays between redox and phosphorylation transduction pathways, which are essential in stomatal movements (Kim et al., 2010).

Conclusions

The present work provides evidence of altered stomatal functioning in plants deficient for several TR types. In Arabidopsis lines lacking class-II GRXs or 2-CysPRXs, the lower stomatal

conductance is associated with reduced growth. However, this cannot be regarded as a general rule since plants deficient in NTRs A and B concomitantly exhibit reduced growth (Fig. S4) and more open stomata (Fig. 3). Taking collectively, the few works reporting a stomatal phenotype resulting from TR deficiency (Hu et al, 2017; Calderon et al, 2018; Mao et al, 2018) and our data highlight the complexity of TR roles in stomata that very likely depend on environmental conditions, developmental stage, and species. This work clearly unveils the participation of plastidial TRs in signaling transduction pathways controlling stomatal closure, and opens new avenues of research to investigate the roles of thiol redox switch in stomatal functioning. In particular, it will be essential to identify TR physiological partners in guard cells, and unravel their integration within the hormone- and ROS-related transduction pathways regulating stomatal movements in response to abiotic environmental stimuli, but also biotic ones, since stomata participate in immune defense mechanisms (Melotto et al., 2006; Montillet and Hirt, 2013). Consistently Pang et al., (2020) recently reported changes in the expression of several *TRX* and *PRX* genes in a GCE fraction following treatment with a bacterial pathogen.

Acknowledgements

We are very grateful to the "Phytotec" platform (CEA, DRF, BIAM) for technical assistance with growth chambers, S. CHIARENZA and N. BROUSSE-POCHON for assistance in growing plants, W. SAINT-AUBIN for technical assistance in experiments, N. BECUWE for molecular characterization of mutants, Dr. I. REITER (CNRS, ECCOREV, O3HP) for equipment supply and advice in porometry experiments, Dr. V. HINOUX (University of Perpignan) for participation in the *trxh3* mutant characterization, Prof. N. ROUHIER (University of Lorraine) for valuable project discussion and M.L. REY for help in formatting the manuscript. D. RONDET acknowledges financial support for a PhD grant (CIFRE contract n° 2014/0798) between CEA and the NIXE Company (Sophia-Antipolis, France), and is

677 grateful to Dr. R. CANAGUIER for helpful discussion. This study is set within the framework
678 of the "Laboratoires d'Excellence (LabEx)" TULIP (ANR-10-LABX-41). Proteomic
679 experiments were partly supported by the Agence Nationale de la Recherche (ProFI grant ANR-
680 10-INBS-08-01).

References

Awad J., Stotz H.U., Fekete A., Krischke M., Engert C., Havaux M., Berger S. & Mueller M.J. (2015). 2-cysteine peroxiredoxins and thylakoid ascorbate peroxidase create a water-water cycle that is essential to protect the photosynthetic apparatus under high light stress conditions. *Plant Physiology,* 167, 1592-1603.

Bashandy T., Guilleminot J., Vernoux T., Caparros-Ruiz D., Ljung K., Meyer Y. & Reichheld J.P. (2010). Interplay between the NADP-linked thioredoxin and glutathione systems in Arabidopsis auxin signaling. *The Plant Cell,* 22, 376-391.

Bender K.W., Wang X., Cheng G.B., Kim H.S., Zielinski R.E. & Huber S.C. (2015). Glutaredoxin AtGRXC2 catalyses inhibitory glutathionylation of Arabidopsis BRI1-associated receptor-like kinase 1 (BAK1*) in vitro*. *Biochemical Journal,* 467, 399-413.

Berry J.A., Beerling D.J. & Franks P.J. (2010). Stomata: key players in the earth system, past and present. *Current Opinion in Plant Biology,* 13, 233-240.

Bréhélin C., Meyer E.H., de Souris J.P., Bonnard G. & Meyer Y. (2003). Resemblance and dissemblance of Arabidopsis type II peroxiredoxins: similar sequences for divergent gene expression, protein localization, and activity. *Plant Physiology,* 132, 2045-2057.

Broin M., Cuiné S., Eymery F. & Rey P. (2002). The plastidic 2-cysteine peroxiredoxin is a target for a thioredoxin involved in the protection of the photosynthetic apparatus against oxidative damage. *The Plant Cell,* 14, 1417-1432.

Calderón A., Sánchez-Guerrero A., Ortiz-Espín A., Martínez-Alcalá I., Camejo D., Jiménez A. & Sevilla F. (2018). Lack of mitochondrial thioredoxin o1 is compensated by antioxidant components under salinity in *Arabidopsis thaliana* plants. *Physiologia Plantarum*, 164, 251-267.

Cerveau D., Henri P., Blanchard L. & Rey P. (2019). Variability in the redox status of plant 2-Cys peroxiredoxins in relation to species and light cycle. *Journal of Experimental Botany*, 70, 5003-5016.

Cerveau D., Kraut A., Stotz H.U., Mueller M.J., Couté Y. & Rey P. (2016a). Characterization of the *Arabidopsis thaliana* 2-Cys peroxiredoxin interactome. *Plant Science*, 252, 30–41.

709 Cerveau D., Ouahrani D., Marok M.A., Blanchard L. & Rey P. (2016b). Physiological
710 relevance of plant 2-Cys peroxiredoxin overoxidation level and oligomerization status. *Plant,*
711 *Cell and Environment,* 39, 103–119.

712 Chen Z. & Gallie D.R. (2004). The ascorbic acid redox state controls guard cell signaling and
713 stomatal movement. *The Plant Cell,* 16, 1143-1162.

714 Costa J.M., Monnet F., Jannaud D., Leonhardt N., Ksas B., Reiter I.M., Pantin F. & Genty B.
715 (2015). Open all night long: the dark side of stomatal control. *Plant Physiology,* 167, 289-294.

716 Cotelle V. & Leonhardt N. (2016). 14-3-3 Proteins in Guard Cell Signaling. *Frontiers in Plant*
717 *Science,* 6, 1210. doi: 10.3389/fpls.2015.01210

718 Courteille A., Vesa S., Sanz-Barrio R., Cazalé A.C., Becuwe-Linka N., Farran I., Havaux M.,
719 Rey P. & Rumeau D. (2013). Thioredoxin m4 controls photosynthetic alternative electron
720 pathways in Arabidopsis. *Plant Physiology,* 161, 508-520.

721 Daloso D. M., Müller K., Obata T., Florian A., Tohge T., Bottcher A., Riondet C., Bariat L.,
722 Carrari F., Nunes-Nesi A., Buchanan B.B., Reichheld J.P., Araújo W.L., & Fernie A.R. (2015).
723 Thioredoxin, a master regulator of the tricarboxylic acid cycle in plant
724 mitochondria. *Proceedings of the National Academy of Sciences USA,* 112, E1392–E1400.
725 https://doi.org/10.1073/pnas.1424840112

726 Day A.M., Brown J.D., Taylor S.R., Rand J.D., Morgan B.A. & Veal E.A. (2012). Inactivation
727 of a peroxiredoxin by hydrogen peroxide is critical for thioredoxin-mediated repair of oxidized
728 proteins and cell survival. *Molecular Cell,* 45, 398-408.

729 Delaunay A., Pflieger D., Barrault M.B., Vinh J. & Toledano M.B. (2002). A thiol peroxidase
730 is an H_2O_2 receptor and redox-transducer in gene activation. *Cell*, 111, 471-481.

731 Duruflé H., Ranocha P., Balliau T., Dunand C. & Jamet E. (2019). Transcriptomic & cell wall
732 proteomic datasets of rosettes and floral stems from five Arabidopsis thaliana ecotypes grown
733 at optimal or sub-optimal temperature. *Data Brief.* 27, 104581. doi: 10.1016/j.dib.2019.104581

734 Farhat D.C., Swale C., Dard C., Cannella D., Ortet P., Barakat M., Sindikubwabo F., Belmudes
735 L., De Bock P.J., Couté Y., Bougdour A. & Hakimi M.A. (2020). A MORC-driven
736 transcriptional switch controls Toxoplasma developmental trajectories and sexual commitment.
737 *Nature Microbiology,* 5, 570-583.

738 da Fonseca-Pereira P., Daloso D.M., Gago J., de Oliveira Silva F.M., Condori-Apfata J.A.,
739 Florez-Sarasa I., Tohge T., Reichheld J.P., Nunes-Nesi A., Fernie A.R. & Araújo W.L. (2019).
740 The mitochondrial thioredoxin system contributes to the metabolic response under drought
741 episodes in Arabidopsis. *Plant Cell Physiology,* 60 213-229. doi: 10.1093/pcp/pcy194

742 da Fonseca-Pereira P., Souza P.V.L., Hou L.Y., Schwab S., Geigenberger P., Nunes-Nesi A.,
743 Timm S., Fernie A.R., Thormählen I., Araújo W.L. & Daloso D.M. (2020). Thioredoxin h2
744 contributes to the redox regulation of mitochondrial photorespiratory metabolism. *Plant, Cell*
745 *and Environment,* 43, 188-208. doi: 10.1111/pce.13640

746 Foyer C.H. & Noctor G. (2016). Stress-triggered redox signalling: what's in pROSpect? *Plant,*
747 *Cell and Environment,* 39, 951-964.

748 Geigenberger P., Thormählen I., Daloso D.M. & Fernie A.R. (2017). The unprecedented
749 versatility of the plant thioredoxin system. *Trends Plant Science,* 22, 249-262.

750 Hägglund P., Finnie C., Yano H., Shahpiri A., Buchanan B.B., Henriksen A. & Svensson B.
751 (2016). Seed thioredoxin h. *Biochimica et Biophysica Acta*, 1864, 974-982.

752 Hetherington A.M. & Woodward F.I. (2003). The role of stomata in sensing and driving
753 environmental change. *Nature,* 424, 901-908.

754 Horrer D., Flütsch S., Pazmino D., Matthews J.S., Thalmann M., Nigro A., Leonhardt N.,
755 Lawson T. & Santelia D. (2016). Blue light induces a distinct starch degradation pathway in
756 guard cells for stomatal opening. *Current Biology*, 26, 362-370. doi: 10.1016/j.cub.2015.12.036

757 Hu Y., Wu Q., Peng Z., Sprague S.A., Wang W., Park J., Akhunov E., Jagadish K.S.V., Nakata
758 P.A., Cheng N., Hirschi K.D. White F.F. & Park S. (2017). Silencing of OsGRXS17 in rice
759 improves drought stress tolerance by modulating ROS accumulation and stomatal closure.
760 *Scientific Reports*, 7, 15950. doi: 10.1038/s41598-017-16230-7

761 Irshad M., Canut H., Borderies G., Pont-Lezica R. & Jamet E. (2008). A new picture of cell
762 wall protein dynamics in elongating cells of Arabidopsis thaliana: confirmed actors and
763 newcomers. *BMC Plant Biology,* 8, 94. doi: 10.1186/1471-2229-8-94

764 Jahan M.S., Ogawa K., Nakamura Y., Shimoishi Y., Mori I.C. & Murata Y. (2008). Deficient
765 glutathione in guard cells facilitates abscisic acid-induced stomatal closure but does not affect
766 light-induced stomatal opening. *Bioscience, Biotechnology and Biochemistry,* 72, 2795-2798.

767 Kim T.H., Böhmer M., Hu H., Nishimura N. & Schroeder J.I. (2010). Guard cell signal
768 transduction network: advances in understanding abscisic acid, CO_2, and Ca^{2+} signaling. *Annual*
769 *Review of Plant Biology,* 61, 561-591.

770 Knuesting J., Riondet C., Maria C., Kruse I., Bécuwe N., König N., Berndt C., Tourrette S.,
771 Guilleminot-Montoya J., Herrero E., Gaymard F., Balk J., Belli G., Scheibe R., Reichheld J.P.,
772 Rouhier N. & Rey P. (2015). Arabidopsis glutaredoxin S17 and its partner NF-YC11/NC2α
773 contribute to maintenance of the shoot apical meristem under long-day photoperiod. *Plant*
774 *Physiology,* 167, 1643-1658.

775 Kollist H., Nuhkat, M. & Roelfsema M.R. (2014). Closing gaps: linking elements that control
776 stomatal movement. *New Phytology,* 203, 44-62.

777 Kwak J.M., Mori I.C., Pei Z.M., Leonhardt N., Torres M.A., Dangl J.L., Bloom R.E., Bodde
778 S., Jones J.D. & Schroeder J.I. (2003). NADPH oxidase AtrbohD and AtrbohF genes function
779 in ROS-dependent ABA signaling in Arabidopsis. *EMBO Journal,* 22, 2623-2633.

780 Lai C.P., Huang L.M., Chen L.O., Chan M.T. & Shaw J.F. (2017). Genome-wide analysis of
781 GDSL-type esterases/lipases in Arabidopsis. *Plant Molecular Biology,* 95,181-197.

782 Lamkemeyer P., Laxa M., Collin V., Li W., Finkemeier I., Schöttler M.A., Holtkamp V.,
783 Tognetti V.B., Issakidis-Bourguet E., Kandlbinder A., Weis E., Miginiac-Maslow M. & Dietz
784 K.J. (2006). Peroxiredoxin Q of Arabidopsis thaliana is attached to the thylakoids and functions
785 in context of photosynthesis. *The Plant Journal,* 45, 968-981.

786 Lawson T. (2009). Guard cell photosynthesis and stomatal function. *New Phytologist,* 181, 13-
787 34.

788 Lee Y., Choi D. & Kende H. (2001). Expansins: ever-expanding numbers and functions.
789 *Current Opinion in Plant Biology,* 4, 527-532.

790 Leonhardt N., Kwak J.M., Robert N., Waner D., Leonhardt G. & Schroeder J.I. (2004).
791 Microarray expression analyses of Arabidopsis guard cells and isolation of a recessive abscisic
792 acid hypersensitive protein phosphatase 2C mutant. *The Plant Cell,* 16, 596-615.

793 Li L., Xu X., Chen C. & Shen Z. (2016). Genome-Wide Characterization and Expression
794 Analysis of the Germin-Like Protein Family in Rice and Arabidopsis. *International Journal of*
795 *Molecular Sciences,* 17, 10. pii: E1622. doi: 10.3390/ijms17101622

796 Lichtenthaler H.K. (1987). Chlorophylls and carotenoids: pigments of photosynthetic
797 biomembranes. *Methods in Enzymology,* 148, 350-382.

798 Liebthal M., Maynard D. & Dietz K.J. (2018). Peroxiredoxins and Redox Signaling in Plants.
799 *Antioxydants & Redox Signaling,* 28, 609-624.

800 Liebthal M., Schuetze J., Dreyer A., Mock H.P., & Dietz K.J. (2020). Redox conformation-
801 specific protein–protein interactions of the 2-ysteine peroxiredoxin in
802 Arabidopsis. *Antioxidants*, *9*, 515.

803 Ma T., Yoo M.J., Zhang T., Liu L., Koh J., Song W.Y., Harmon A.C., Sha W. & Chen S.
804 (2018). Characterization of thiol-based redox modifications of *Brassica napus* SNF1-related
805 protein kinase 2.6-2C. *FEBS Open Biology,* 8, 628-645.

806 Mao X., Zheng, Y., Xiao K., Wei Y., Zhu Y., Cai Q., Chen L., Xie H. & Zhang, J. (2018).
807 OsPRX2 contributes to stomatal closure and improves potassium deficiency tolerance in rice.
808 *Biochemical and Biophysical Research Communications,* 495, 461-467.

809 Melotto M., Underwood W., Koczan J., Nomura K. & He S.Y. (2006). Plant stomata function
810 in innate immunity against bacterial invasion. *Cell,* 126, 969–980.

811 Merlot S., Leonhardt N., Fenzi F., Valon C., Costa M., Piette L., Vavasseur A., Genty B., Boivin
812 K., Müller A., Giraudat J. & Leung J. (2007). Constitutive activation of a plasma membrane
813 $H(^{+})$-ATPase prevents abscisic acid-mediated stomatal closure. *EMBO Journal,* 26, 3216-3226.

814 Meyer Y., Belin C., Delorme-Hinoux V., Reichheld J.P. & Riondet C. (2012). Thioredoxin and
815 glutaredoxin systems in plants: molecular mechanisms, crosstalks, and functional significance.
816 *Antioxidants & Redox Signaling,* 17, 1124-1160.

817 Miao Y., Lv D., Wang P., Wang X.C., Chen J., Miao C. & Song C.P. (2006). An Arabidopsis
818 glutathione peroxidase functions as both a redox transducer and a scavenger in abscisic acid
819 and drought stress responses. *The Plant Cell,* 18, 2749-2766.

820 Montillet J.L. & Hirt H. (2013). New check points in stomatal defense. *Trends in Plant Science,*
821 18, 295-297. doi: 10.1016/j.tplants.2013.03.007

822 Montrichard F., Alkhalfioui F., Yano H., Vensel W.H., Hurkman W.J. & Buchanan B.B.
823 (2009). Thioredoxin targets in plants: the first 30 years. *Journal of Proteomics,* 72, 452-474.

Murata Y., Mori I.C. & Munemasa S. (2015). Diverse stomatal signaling and the signal integration mechanism. *Annual Review of Plant Biology,* 66, 369-392.

Naranjo B., Diaz-Espejo A., Lindahl M. & Cejudo F.J. (2016). Type-f thioredoxins have a role in the short-term activation of carbon metabolism and their loss affects growth under short-day conditions in *Arabidopsis thaliana*. *Journal of Experimental Botany,* 67, 1951-1964.

Navrot N., Collin V., Gualberto J., Gelhaye E., Hirasawa M., Rey P., Knaff D.B, Issakidis E., Jacquot J.P. & Rouhier N. (2006). Plant glutathione peroxidases are functional peroxiredoxins distributed in several subcellular compartments and regulated during biotic and abiotic stresses. *Plant Physiology,* 142, 1364-1379.

Ortiz-Espín A., Iglesias-Fernández R., Calderón A., Carbonero P., Sevilla F. & Jiménez. A. (2017). Mitochondrial AtTrxo1 is transcriptionally regulated by AtbZIP9 and AtAZF2 and affects seed germination under saline conditions. *Journal of Experimental Botany,* 68, 1025-1038.

Pang Q., Zhang T., Zhang A., Lin C., Kong W. & Chen S. (2020). Proteomics and phosphoproteomics revealed molecular networks of stomatal immune responses. *Planta,* 252, 66. doi: 10.1007/s00425-020-03474-3.

Papadakis A.K. & Roubelakis-Angelakis K.A. (1999). The generation of active oxygen species differs in Nicotiana and Vitis plant protoplasts. *Plant Physiology,* 121,197–205.

Park S.K., Jung Y.J., Lee J.R., Lee Y.M., Jang H.H., Lee S.S., Park J.H., Kim S.Y., Moon J.C., Lee S.Y., Chae H.B., Shin M.R., Jung J.H., Kim M.G., Kim W.Y., Yun D.J., Lee K.O. & Lee S.Y. (2009). Heat-shock and redox-dependent functional switching of an h-type Arabidopsis thioredoxin from a disulfide reductase to a molecular chaperone. *Plant Physiology,* 150, 552-561.

Poole L.B., Hall A. & Nelson K.J. (2011). Overview of peroxiredoxins in oxidant defense and redox regulation. *Current Protocols in Toxicology,* 7, 9. doi: 10.1002/0471140856.tx0709s49.

Pulido P., Spínola M.C., Kirchsteiger K., Guinea M., Pascual M.B., Sahrawy M., Sandalio L.M., Dietz K.J., González M. & Cejudo F.J. (2010). Functional analysis of the pathways for 2-Cys peroxiredoxin reduction in *Arabidopsis thaliana* chloroplasts. *Journal of Experimental Botany,* 61, 4043-4054.

Reichheld J.P., Khafif M., Riondet C., Droux M., Bonnard G. & Meyer Y. (2007). Inactivation of thioredoxin reductases reveals a complex interplay between thioredoxin and glutathione pathways in Arabidopsis development. *The Plant Cell,* 19, 1851-1865.

Reichheld J.P., Mestres-Ortega D., Laloi C. & Meyer Y. (2002). The multigenic family of thioredoxin *h* in *Arabidopsis thaliana*: specific expression and stress response. *Plant Physiology and Biochemistry,* 40, 685-690.

Rey P., Becuwe N., Barrault M.B., Rumeau D., Havaux M., Biteau B. & Toledano M.B. (2007). The *Arabidopsis thaliana* sulfiredoxin is a plastidic acid reductase involved in the photooxidative stress response. *The Plant Journal,* 49, 505-514.

Rey P., Becuwe N., Tourrette S. & Rouhier N. (2017). Involvement of Arabidopsis glutaredoxin S14 in the maintenance of chlorophyll content. *Plant, Cell and Environment,* 40, 2319–2332.

Rey P., Cuiné S., Eymery F., Garin J., Court M., Jacquot J.P., Rouhier N. & Broin M. (2005). Analysis of the proteins targeted by CDSP32, a plastidic thioredoxin participating in oxidative stress responses. *The Plant Journal,* 41, 31-42.

Rey P. & Tarrago L. (2018). Physiological roles of plant methionine sulfoxide reductases in redox homeostasis and signaling. *Antioxidants (Basel)*, 7(9). pii: E114. doi: 10.3390/antiox7090114

Rhee S.G. & Woo H.A. (2011). Multiple functions of peroxiredoxins: peroxidases sensors and regulators of the intracellular messenger H_2O_2 and protein chaperones. *Antioxidants & Redox Signaling,* 15, 781-794.

Rodrigues O., Reshetnyak G., Grondin A., Saijo Y., Leonhardt N., Maurel C. & Verdoucq L. (2017). Aquaporins facilitate hydrogen peroxide entry into guard cells to mediate ABA- and pathogen-triggered stomatal closure. *Proceedings of the National Academy of Sciences USA,* 114, 9200-9205.

Rouhier N., Cerveau D., Couturier J., Reichheld J.P. & Rey P. (2015). Involvement of thiol-based mechanisms in plant development. *Biochemical et Biophysical Acta,* 1850, 1479-1496.

Rouhier N., Gelhaye E., Gualberto J.M., Jordy M.N., De Fay E., Hirasawa M., Duplessis S., Lemaire S.D., Frey P., Martin F., Manieri W., Knaff D.B. & Jacquot J.P. (2004). Poplar peroxiredoxin Q. A thioredoxin-linked chloroplast antioxidant functional in pathogen defense. *Plant Physiology,* 134, 1027-1038.

Rouhier N., Lemaire S.D. & Jacquot J.P. (2008). The role of glutathione in photosynthetic organisms: emerging functions for glutaredoxins and glutathionylation. *Annual Review of Plant Biology,* 59, 143-166.

Rouhier N., Villarejo A., Srivastava M., Gelhaye E., Keech O., Droux M., Finkemeier I., Samuelsson G., Dietz K.J., Jacquot J.P. & Wingsle G. (2005). Identification of plant glutaredoxin targets. *Antioxidants & Redox Signaling,* 7, 919-929.

Roux B. & Leonhardt N. (2018). The regulation of ion channels and transporters in the guard cell. *Advances in Botanical Research,* 87, 171-214. doi.org/10.1016/bs.abr.2018.09.013.

Salvetti A., Couté Y., Epstein A., Arata L., Kraut A., Navratil V., Bouvet P. & Greco A. (2016). Nuclear functions of nucleolin through global proteomics and interactomic approaches. *Journal of Proteome Research,* 15, 1659-1669.

Schürmann P. & Buchanan B.B. (2008) The ferredoxin/thioredoxin system of oxygenic photosynthesis. *Antioxidants & Redox Signaling,* 10, 1235–1274.

Schwanhaüsser B., Busse D., Li N., Dittmar G., Schuchhardt J., Wolf J., Chen W. & Selbach M. (2011). Global quantification of mammalian gene expression control. *Nature,* 473, 337-342.

Shimazaki K., Doi. M., Assmann S.M. & Kinoshita T. (2007). Light regulation of stomatal movement. *Annual Review of Plant Biology,* 58, 219-47.

Showalter A.M., Keppler B., Lichtenberg J., Gu D. & Welch L.R. (2010). A bioinformatics approach to the identification, classification, and analysis of hydroxyproline-rich glycoproteins. *Plant Physiology,* 153, 485-513.

Sierla M., Waszczak C., Vahisalu T. & Kangasjärvi J. (2016). Reactive oxygen species in the regulation of stomatal movements. *Plant Physiology,* 171, 1569-1580.

Song Y., Miao Y. & Song C.P. (2014). Behind the scenes: the roles of reactive oxygen species in guard cells. *New Phytologist,* 201, 1121-1140.

Stöcker S., Maurer M., Ruppert T. & Dick T.P. (2017). A role for 2-Cys peroxiredoxins in facilitating cytosolic protein thiol oxidation. *Nature Chemical Biology,* 14, 148-155.

Sweat T.A. & Wolpert T.J. (2007). Thioredoxin h5 is required for victorin sensitivity mediated by a CC-NBS-LRR gene in Arabidopsis. *The Plant Cell*, 19, 673-687.

911 Tada Y., Spoel S.H., Pajerowska-Mukhtar K., Mou Z., Song J., Wang C., Zuo J. & Dong X.
912 (2008). Plant immunity requires conformational changes of NPR1 via S-nitrosylation and
913 thioredoxins. *Science,* 321, 952-956.

914 Tarrago L., Laugier E. & Rey P. (2009). Protein-repairing methionine sulfoxide reductases in
915 photosynthetic organisms: gene organization, reduction mechanisms, and physiological roles.
916 *Molecular Plant,* 2, 202-217.

917 Tseng T.S., Whippo C., Hangarter R.P. & Briggs W.R. (2012). The role of a 14-3-3 protein in
918 stomatal opening mediated by PHOT2 in Arabidopsis. *The Plant Cell*, 24, 1114-1126.

919 Tyanova S., Temu T. & Cox J. (2016). The MaxQuant computational platform for mass
920 spectrometry-based shotgun proteomics. *Nature Protocols,* 11, 2301-2319.

921 Valerio C., Costa A., Marri L., Issakidis-Bourguet E., Pupillo P., Trost P. & Sparla F. (2011).
922 Thioredoxin-regulated beta-amylase (BAM1) triggers diurnal starch degradation in guard cells,
923 and in mesophyll cells under osmotic stress. *Journal of Experimental Botany,* 62, 545-555.

924 Vieira Dos Santos C. & Rey P. (2006). Plant thioredoxins are key actors in oxidative stress
925 response. *Trends in Plant Science,* 11, 329-334.

926 Wang P., Du Y., Hou Y.J., Zhao Y., Hsu C.C., Yuan F., Zhu X., Tao W.A., Song C.P. & Zhu
927 J.K. (2015). Nitric oxide negatively regulates abscisic acid signaling in guard cells by S-
928 nitrosylation of OST1. *Proceedings of the National Academy of Sciences USA,* 112, 613-618.

929 Wang W., Vignani R., Scali M. & Cresti M. (2006). A universal and rapid protocol for protein
930 extraction from recalcitrant plant tissues for proteomic analysis. *Electrophoresis,* 27, 2782-
931 2786.

932 Wei P.C., Zhang X.Q., Zhao P. & Wang X.C. (2011). Regulation of stomatal opening by the
933 guard cell expansin AtEXPA1. *Plant Signaling Behavior*, 6, 740-742.

934 Wieczorek S., Combes F., Lazar C., Giai Gianetto Q., Gatto L., Dorffer A., Hesse A.M., Couté
935 Y., Ferro M., Bruley C. & Burger T. (2017). DAPAR & ProStaR: software to perform statistical
936 analyses in quantitative discovery proteomics. *Bioinformatics,* 33, 135-136.

937

Winter D., Vinegar B., Nahal H., Ammar R., Wilson G.V. & Provart N.J. (2007). An "Electronic Fluorescent Pictograph" browser for exploring and analyzing large-scale biological data sets. *PLoS One*, 2, e718. doi: 10.1371/journal.pone.0000718.

Woo H.A., Yim S.H., Shin D.H., Kang D., Yu D.Y. & Rhee S.G. (2010). Inactivation of peroxiredoxin I by phosphorylation allows localized H_2O_2 accumulation for cell signaling. *Cell,* 140, 517-528.

Wu F.H., Shen S.C., Lee L.Y., Lee S.H., Chan M.T. & Lin C.S. (2009). Tape-Arabidopsis Sandwich - a simpler Arabidopsis protoplast isolation method. *Plant Methods,* 5, 16.

Yang Y., Costa A., Leonhardt N., Siegel R.S. & Schroeder J.I. (2008). Isolation of a strong Arabidopsis guard cell promoter and its potential as a research tool. *Plant Methods,* 4, 6.

Yoshida K., Hara A., Sugiura K., Fukaya Y. & Hisabori T. (2018). Thioredoxin-like2/2-Cys peroxiredoxin redox cascade supports oxidative thiol modulation in chloroplasts. *Proceedings of the National Academy of Sciences USA,* 115, E8296-E8304.

Zhang X.Q., Wei P.C., Xiong Y.M., Yang Y., Chen J. & Wang X.C. (2011). Overexpression of Arabidopsis alpha-expansin gene AtEXPA1 accelerates stomatal opening by decreasing the volumetric elastic modus. *Plant Cell Reports,* 30, 27-36.

Zhang T., Zhu M., Zhu N., Strul J.M., Dufresne C.P., Schneider J.D., Harmon A.C. & Chen S. (2016). Identification of thioredoxin targets in guard cell enriched epidermal peels using cysTMT proteomics. *Journal of Proteomics,* 133, 48-53.

Zhao Z., Stanley B.A., Zhang W. & Assmann S.M. (2010). ABA-regulated G protein signaling in Arabidopsis guard cells: a proteomic perspective. *Journal of Proteome Research,* 9, 1637-1647.

Zhao Z., Zhang W., Stanley B.A. & Assmann S.M. (2008). Functional proteomics of Arabidopsis thaliana guard cells uncovers new stomatal signaling pathways. *The Plant Cell*, 12, 3210-3226.

Zhu M., Dai S., McClung S., Yan X. & Chen S. (2009). Functional differentiation of *Brassica napus* guard cells and mesophyll cells revealed by comparative proteomics. *Molecular Cell Proteomics*, 8, 752-766.

966 Zhu M., Simons B., Zhu N., Oppenheimer D.G. & Chen S. (2010). Analysis of abscisic acid
967 responsive proteins in *Brassica napus* guard cells by multiplexed isobaric tagging. *Journal of*
968 *Proteomics,* 73, 790-805.

969 Zhu M., Zhang T., Ji W., Silva-Sanchez C., Song W.Y., Assmann S.M., Harmon A.C. & Chen
970 S. (2017). Redox regulation of a guard cell SNF1-related protein kinase in *Brassica napus*, an
971 oilseed crop. *Biochemical Journal,* 474, 2585-2599.

972 Zhu M., Zhu N., Song W.Y., Harmon A.C., Assmann S.M. & Chen S. (2014). Thiol-based
973 redox proteins in abscisic acid and methyl jasmonate signaling in *Brassica napus* guard cells.
974 *The Plant Journal,* 78, 491-515.

975

AGI Number	Protein ID	Description	GCE	L	GCE-L	R	GC proteomics	GC/M transcript ratio > 2	Reference
AT5G26000	P37702	Myrosinase 1 *	31,43	29,21	2,22	**4,66**	**X**	●	[54]
AT1G69530	Q9C554	Expansin-A1 *	29,30	24,39	4,91	**30,1**		●	[48]; [53]
AT3G53420	P43286	Aquaporin PIP2-1 #	29,05	29,17	-0,12	0,92	**X**		[43]
AT2G18960	P20649	ATPase 1 #	27,77	24,99	2,78	**6,87**	**X**	●	[21]
AT5G56030	P55737	Heat shock protein 90-2 *	27,46	27,15	0,32	1,25	**X**	●	[6]
AT5G10450	F4KGV2	G-box regulating factor 6 *	27,36	23,98	3,38	**10,4**			[39]
AT5G67500	Q9FJX3	Voltage-dependent anion channel 2 #	27,23	24,61	2,62	**6,15**	**X**	●	[27]
AT1G70410	Q94CE4	Beta carbonic anhydrase 4 *	27,08	25,87	1,21	**2,31**	**X**		[15]
AT3G15730	Q38882	Phospholipase D alpha 1 *	26,60	25,83	0,77	**1,71**	**X**	●	[41]
AT5G02500	F4KCE5	Heat shock cognate 70 kDa protein 1 *	26,53	27,09	-0,57	0,68	**X**	●	[6]
AT1G12840	Q9SDS7	V-type proton ATPase subunit C #	26,17	24,86	1,31	**2,48**		●	[1]; [18]
AT1G15690	P31414	Vacuolar membrane proton pump 1 #	25,96	26,85	-0,89	0,54	**X**		[3]
AT1G11260	P23586	Sugar transport protein 1 #	25,70	21,16	4,54	**23,3**	**X**	●	[35]; [31]
AT4G29130	Q42525	Hexokinase-1 §	25,00	24,43	0,57	1,48		●	[24]
AT3G18490	Q9LS40	Aspartic protease in guard cell 1*	24,98	23,42	1,57	**2,96**		●	[51]
AT1G04110	O64495	Subtilisin-like protease SBT1.2 ¤	24,83	15,90	8,93	**489**			[42]
AT4G05590	Q8L7H8	Mitochondrial pyruvate carrier 3 *	24,73	**15,18**	9,55	**GCE**			[52]; [35]
AT5G57110	Q9LF79	Calcium-transporting ATPase 8 #	24,37	22,47	1,89	**3,72**	**X**		[50]
AT4G03560	Q94KI8	Two pore calcium channel protein 1 #	24,31	20,57	3,74	**13,4**		●	[34]
AT3G02880	Q9M8T0	Probable inactive receptor kinase §	23,81	23,47	0,33	1,26	**X**		[18]
AT5G46790	Q8VZS8	Abscisic acid receptor PYL1 !	23,59	22,21	1,38	**2,60**		●	[45]
AT1G13320	Q38951	Protein phosphatase 2A subunit A3 §	23,57	20,06	3,51	**11,4**			[26]
AT4G23650	Q42479	Calcium-dependent protein kinase 3 §	23,32	24,62	-1,30	0,41	**X**		[30]
AT4G30190	P19456	ATPase 2, plasma membrane-type #	23,25	20,95	2,30	**4,92**	**X**	●	[46]
AT2G26040	O80992	Abscisic acid receptor PYL2 !	22,92	**15,18**	7,74	**GCE**	**X**	●	[45]
AT1G55020	Q06327	Linoleate 9S-lipoxygenase 1 *	22,91	20,35	2,56	**5,90**		●	[29]
AT1G52340	Q9C826	Xanthoxin dehydrogenase *	22,89	21,21	1,68	**3,20**		●	[49]
AT2G46070	Q8GYQ5	Mitogen-activated protein kinase 12 §	22,81	17,65	5,16	**35,8**	**X**	●	[20]
AT5G50000	Q9FGB1	Protein kinase superfamily protein §	22,80	21,03	1,76	**3,39**	**X**	●	[14]
AT4G17870	O49686	Abscisic acid receptor PYR1 !	22,73	21,86	0,87	**1,83**		●	[33]
AT4G35790	Q9C5Y0	Phospholipase D delta *	22,46	20,88	1,58	**2,99**	**X**	●	[41]
AT5G13630	Q9FNB0	Magnesium-chelatase subunit ChlH *	21,77	24,15	-2,38	0,19			[40]
AT2G43350	O22850	Glutathione peroxidase 3 *	21,56	**15,18**	6,38	**GCE**		●	[28]
AT2G43790	Q39026	Mitogen-activated protein kinase 6 §	21,29	19,99	1,30	**2,46**		●	[29]
AT2G13540	Q9SIU2	Nuclear cap-binding protein subunit 1 *	21,21	18,32	2,89	**7,41**			[17]
AT3G53720	Q9M353	Cation/H(+) antiporter 20 #	21,21	15,18	6,03	**GCE**	**X**	●	[32]
AT1G32080	Q9FVQ4	Plastidal glycolate/glycerate translocator#	21,19	23,68	-2,48	0,18			[7]
AT5G40890	P92941	Chloride channel protein CLC-a #	20,92	19,53	1,40	**2,63**	**X**	●	[47]
AT5G24520	Q9XGN1	TRANSPARENT TESTA GLABRA 1 ¤	20,81	18,93	1,87	**3,66**		●	[9]
AT1G28490	Q946Y7	Syntaxin-61 *	20,64	18,52	2,12	**4,35**		●	[55]
AT4G14480	O23304	Serine/threonine-protein kinase BLUS1 §	20,56	**15,18**	5,38	**41,6**	**X**	●	[38]
AT5G49890	Q96282	Chloride channel protein CLC-c #	20,22	**15,18**	5,04	**GCE**		●	[22]
AT4G04720	Q9ZSA2	Calcium-dependent protein kinase 21 §	20,15	20,73	-0,57	0,67			[10]
AT1G23200	O49298	Pectinesterase/pectinesterase inhibitor 6 *	19,84	**15,18**	4,66	**GCE**		●	[2]
AT3G08550	Q9C9Z9	Glycosyltransferase-like KOBITO 1 *	19,46	19,62	-0,15	0,90		●	[25]
AT4G08920	Q43125	Cryptochrome-1 ¤	19,35	18,73	0,63	**1,55**			[23]
AT4G17615	Q9LTB8	Calcineurin B-like protein 1 *	19,31	**15,18**	4,13	**GCE**			[5]
AT5G63870	Q9FN02	Serine/threonine-protein phosphatase 7 §	19,12	19,04	0,07	1,05		●	[37]

AT1G04400	Q96524	Cryptochrome-2 ¤	19,01	**15,18**	3,83	**GCE**		●	[4]
AT1G12110	Q05085	Nitrate transporter 1.1 #	18,76	17,50	1,26	**2,39**		●	[11]
AT2G36850	Q9SJM0	Callose synthase 10 ¤	18,77	16,02	2,75	**6,72**		●	[12]
AT1G49040	Q8RXA7	DENN-domain WD-repeat protein ¤	18,69	17,87	0,82	**1,77**	**X**		[8]
AT3G45640	Q39023	Mitogen-activated protein kinase 3 §	17,93	17,01	0,92	**1,89**			[44]
AT1G35670	Q39016	Calcium-dependent protein kinase 2 §	17,83	16,81	1,03	**2,04**			[16]
AT1G62400	Q2MHE4	Serine/threonine-protein kinase HT1 §	17,44	**15,18**	2,26	**GCE**		●	[13]
AT2G18790	P42497	Phytochrome ¤	17,43	19,21	-1,78	0,29		●	[23]

Table 1. List of proteins present in the guard cell-enriched fraction and playing a role in stomatal functioning and development.

Proteins are ranked from the most abundant to the less in the GCE fraction. Bold lines separate quartiles. In GCE and L columns are reported $\log_2$ of imputed normiBAQ that reflect relative abundance of each protein in guard cell-enriched and leaf fractions, respectively. R represents protein abundance ratio in the GC-enriched fraction epidermis relative to leaf fraction and is equal to $2^{(E-L)}$. Bold R value, protein having a value > 1.5 and thus more abundant in the GCE fraction than in the L fraction. **GCE**, protein found only in the guard cell-enriched fraction Underlined L value, only 1 peptide detected; bold L value, no peptide detected. **X**, Protein identified in Arabidopsis guard cell proteomics by Zhao et al., (2008; 2010). ●, Transcript ratio, GC protoplast level/mesophyll protoplast level, higher than 2 (Yang et al., 2008). Classification of proteins: §, kinases and phosphatases involved in stomatal movements; #, Ion channels, transporters and pumps involved in stomatal movements;!, ABA receptors; ¤, Proteins involved in regulation of stomatal development and patterning ; *, Enzymes and other protein functions. References are listed in Table S6.

AGI Number	Protein ID	Description	Name	GCE	L	GCE-L	R	GC proteomics
AT3G26060	Q9LU86	Peroxiredoxin Q	PRXQ	28,20	29,82	-1,62	0,33	
AT3G11630	Q96291	2-Cys peroxiredoxin A	2-CysPrxA	27,71	27,09	0,63	**1,55**	**X**
AT1G65980	Q9XEX2	Peroxiredoxin IIB	Prx IIB	26,14	23,27	2,87	**7,29**	
AT3G06050	Q9M7T0	Peroxiredoxin IIF	Prx IIF	25,99	25,28	0,71	**1,64**	**X**
AT2G17420	Q39242	NADPH-thioredoxin reductase A	NTRA	25,94	24,01	1,92	**3,79**	
AT3G52960	Q949U7	Peroxiredoxin IIE	Prx IIE	25,61	27,37	-1,76	0,30	**X**
AT5G42980	Q42403	Thioredoxin h3	TRX h3	25,00	22,90	2,10	**4,29**	**X**
AT4G11600	O48646	Glutathione peroxidase 6	GPX6	24,44	23,79	0,65	**1,56**	**X**
AT5G06290	Q9C5R8	2-Cys peroxiredoxin B	2-CysPrxB	24,19	25,08	-0,88	0,54	**X**
AT5G07460	Q9LY15	Peptide methionine sulfoxide reductase A2	MSRA2	24,17	22,55	1,62	**3,08**	**X**
AT1G60420	O80763	Nucleoredoxin 1	NRX1	23,95	21,82	2,13	**4,38**	
AT4G35460	Q39243	NADPH-thioredoxin reductase B	NTRB	23,93	20,25	3,69	**12,9**	
AT4G25130	P54150	Peptide methionine sulfoxide reductase A4	MSRA4	23,87	26,50	-2,63	0,16	**X**
AT2G25080	P52032	Glutathione peroxidase 1	GPX1	23,20	23,81	-0,61	0,65	
AT2G31570	O04922	Glutathione peroxidase 2	GPX2	22,76	20,98	1,78	**3,43**	**X**
AT3G06730	Q9M7X9	Thioredoxin z	TRX z	22,71	**15,18**	7,53	**GCE**	
AT5G39950	Q38879	Thioredoxin h2	TRX h2	22,43	19,63	2,80	**6,96**	
AT4G03520	Q9SEU8	Thioredoxin m2	TRX m2	22,17	26,87	-4,70	0,04	**X**
AT2G38270	Q8H7F6	Glutaredoxin S16	GRXS16	22,14	24,32	-2,18	0,22	**X**
AT2G41680	O22229	NADPH-thioredoxin reductase C	NTRC	22,09	26,15	-4,06	0,06	
AT3G02730	Q9XFH8	Thioredoxin f1	TRX f1	21,96	25,88	-3,93	0,07	
AT3G08710	Q9C9Y6	Thioredoxin h9	TRX h9	21,81	**15,18**	6,63	**GCE**	
AT3G15660	Q8LBK6	Glutaredoxin S15,	GRXS15	21,80	**15,18**	6,62	**GCE**	
AT4G04950	Q9ZPH2	Glutaredoxin S17	GRXS17	21,72	20,97	0,75	**1,68**	
AT3G15360	Q9SEU6	Thioredoxin m4	TRX m4	21,72	26,37	-4,66	0,04	**X**
AT1G03680	O48737	Thioredoxin m1	TRX m1	21,65	25,86	-4,21	0,05	
AT3G63080	Q9LYB4	Glutathione peroxidase 5	AtGPX5	21,59	22,49	-0,89	0,54	
AT2G43350	O22850	Glutathione peroxidase 3	AtGPX3	21,56	**15,18**	6,38	**355**	
AT1G76080	Q9SGS4	Chloroplastic Drought Stress 32-kDa Protein	TRX CDSP32	21,41	25,66	-4,25	0,05	
AT4G29670	Q8LCT3	Atypical cysteine/histidine-rich thioredoxin 2	ACHT2	21,39	23,63	-2,24	0,21	
AT4G28730	Q8GWS0	Glutaredoxin C5	GRXC5	21,26	23,56	-2,30	0,20	
AT2G35010	O64764	Thioredoxin o1	TRX o1	20,99	20,43	0,55	1,47	**X**
AT1G11530	Q8LDI5	Thioredoxin-like, Mono-cysteine 1	TRX CxxS1	20,89	18,83	2,06	**4,21**	
AT4G21860	Q9C5C8	Methionine sulfoxide reductase B2	MSRB2	20,78	24,26	-3,48	0,09	
AT3G17880	Q8VWG7	Tetratricoredoxin	TDX	20,61	**15,18**	5,43	**GCE**	
AT5G08410	Q8LBP6	Ferredoxin/thioredoxin reductase subunit A2	FTRA2	20,27	21,52	-1,25	0,42	
AT1G07700	Q9C5C5	Thioredoxin-like, Lilium-type thioredoxin 6	Lilium6	20,08	**15,18**	4,90	**GCE**	
AT2G18030	Q9SL43	Methionine sulfoxide reductase A5	MSRA5	20,07	20,31	-0,24	0,84	
AT4G37200	O23166	Thioredoxin High Chlorophyll Fluorescence 164	TRX HCF164	19,72	23,43	-3,71	0,08	

1009
1010

Table 2. List of thiol reductases identified in the guard cell-enriched fraction

Proteins are ranked from the most abundant to the less in the GCE fraction. Bold lines separate quartiles. In GCE and L columns are reported $\log_2$ of imputed normiBAQ that reflect relative abundance of each protein in guard cell-enriched and leaf fractions, respectively. R represents protein abundance ratio in the GC-enriched fraction epidermis relative to leaf fraction and is equal to $2^{(E-L)}$. Bold R value, protein having a value > 1.5 and thus more abundant in the GCE fraction than in the L fraction. **GCE**, protein found only in the guard cell enriched-fraction. Bold L value, no peptide detected. **X**, Protein identified in Arabidopsis guard cell proteomics by Zhao et al., (2008; 2010).

Figure legends

Figure 1. Western blot analysis of the abundance of thiol reductases in extracts from a guard cell-enriched fraction

A. Coomassie Blue-stained gel of SDS-PAGE separated proteins from leaf blades (L) and GCE fractions. The arrows indicate proteins noticeably more abundant in the GCE fraction. LSU and SSU, large and small RubisCO subunits, respectively. **B.** Western blot analysis of RubisCO subunits and of various types of thiol reductases in L and GCE fractions. Blots (20 to 30 µg proteins per lane, depending on the serum used, for both fractions) were probed using antibodies raised against RubisCO (1:10,000), TRX h3 (1:20,000), 2-CysPRX (1:10,000) 2-CysPRX-Ox, hyperoxidized 2-CysPRX (1:4000), PRXQ (1:1000), PRX-IIE (1:10,000) PRXII-B (1:20,000) and GRXS14 (1:800). For the latter, the asterisk points to a non-specific band and the two arrows indicate two GRX redox forms.

Figure 2. Functional categorization (GO Cellular Component) of proteins identified in guard cell-enriched and leaf fractions.

Functional categorization was performed using of the GO annotation retrieval tool available on the site TAIR: https://www.arabidopsis.org/tools/bulk/go/index.jsp. Analysis was performed on genes encoding the 25% most abundant proteins of each sample (in GCE fraction, 1102 proteins having a Log2(iBAQ) ≥ 24.06 and in leaf fraction 913 proteins with Log2(iBAQ) ≥ 23.97).

Figure 3. Stomatal phenotype of the Arabidopsis *ntra ntrb* mutant

A. Stomatal density. **B**. Stomatal index. Data for **A** and **B** are means ± SD of 12 independent values using peeled epidermis from three leaves per genotype. Plants were grown for 4 weeks in control conditions: moderate light (200 µmol photons.m^{-2}.s^{-1}) and short photoperiod (8 h) at 22°C. **C.** Stomatal conductance measurements using porometry. Measurements of the water efflux from leaf abaxial side were performed on plants grown for 6 weeks in control conditions. Conductance values are means ± SD of twelve average values per genotype originating from independent plants (8 measurements per plant for each genotype per experiment). ***, significantly different from the WT value with $P < 0.001$ (*t*-test). **D**. and **E**. Infrared thermal imaging. Plants were dark-adapted. False colored infrared images of 6-week-old plants grown in control conditions. The color scale on the right shows increasing temperature from purple to yellow. Pictures were taken at the end of the night period two hours before the light period. As a control, the *ost2-2D* mutant was used and shown to exhibit lower leaf temperature due to open stomata in the dark (Merlot et al., 2007). *ntra ntrb*, double *ntra ntrb* mutant plants.

Figure 4. Stomatal phenotype of Arabidopsis mutants deficient in plastidial PRXs

A. Stomatal density. **B**. Stomatal index. Data for **A** and **B** are means ± SD of 12 independent values using peeled epidermis from three leaves per genotype. Plants were grown for 4 weeks in control conditions: moderate light (200 µmol photons.m^{-2}.s^{-1}) and short photoperiod (8 h) at 22°C. **C.** Stomatal conductance measurements using porometry. Measurements of the water efflux from leaf abaxial side were performed on plants grown for 6 weeks in control conditions. Conductance values are means ± SD of eight average values per genotype originating from independent plants (8 measurements per plant for each genotype per experiment). **, significantly different from the WT value with $P < 0.01$ (*t*-test). **D**. and **E.** Infrared thermal imaging. Plants were dark-adapted. False colored infrared images of 6-week-old plants grown in control conditions. The color scale on the right shows increasing temperature from purple to yellow. Pictures were taken at the end of the night period two hours before the light period. *2cprx*, double *2cysprxa 2cysprxb* mutant plants; *prxq,* knockout *PRXQ* plants.

Figure 5. Stomatal phenotype of Arabidopsis lines modified for plastidial type-II GRXs. A. Stomatal density. **B**. Stomatal index. Data for **A** and **B** are means ± SD of 12 independent values using peeled epidermis from three leaves per genotype. Plants were grown for 4 weeks in control conditions: moderate light (200 µmol photons.m^{-2}.s^{-1}) and short photoperiod (8 h) at 22°C. **C.** Stomatal conductance measurements using porometry. Measurements of the water efflux from leaf abaxial side were performed on plants grown for 6 weeks in control conditions. Conductance values are means ± SD of at least 17 average values per genotype originating from independent plants (8 measurements per plant for each genotype per experiment). ***, significantly different from the WT value with $P < 0.001$ (*t*-test). **D**. and **E**. Infrared thermal imaging. Plants were dark-adapted. False colored infrared images of 6-week-old plants grown in control conditions. Pictures were taken at the end of the night period two hours before the light period. The color scale on the right shows increasing temperature from purple to yellow. As a control, the *ost2-2D* mutant was used and shown to exhibit lower leaf temperature due to open stomata in the dark (Merlot et al., 2007). KI1 and KI2, independent *grxS14* GRXS16-RNAi lines; OE1 and OE2, independent *GRXS14*-overexpressing lines.

Figure 6. Effect of ABA and H_2O_2 on stomatal aperture in Arabidopsis mutants deficient in cytosolic NTRs, plastidial 2Cys-PRXs or plastidial type-II GRXs.

Stomatal aperture measurements in response to ABA concentrations of 0.5, 1, 10 and 100 µM (**A**-**B**) or to H_2O_2 concentrations of 10, 100 and 1000 µM (**C**-**D**) in light-treated epidermis. Data in panels **B** and **D** were calculated from the original raw data reported in panels **A** and **C**, respectively, and represent the inhibitions of stomatal aperture due to the treatments expressed in percents of that measured in light alone. Data represent means ± SD of 2 independent experiments with 60 measurements per genotype and treatment. Means were compared with

the ANOVA test, and letters represent groups of means not statistically different (P<0.05). *2cprx*, double *2cysprxa 2cysprxb* mutant plants; KI1 and KI2, independent *grxS14* GRXS16-RNAi lines; *ntra ntrb*, double *ntra ntrb* mutant plants.

Figure 7. Model for positioning putative roles of plastidial 2-CysPRXs and type-II GRXs in the signaling network governing stomatal closure. Based on the results gained on epidermal peels showing modified responses of mutants to ABA and H_2O_2 and the known biochemical functions of these enzymes, we propose that they participate in H_2O_2-related transduction pathways. 2-CysPRXs might scavenge H_2O_2 within plastid or promote oxidation of partners that remain to be identified and are involved, when oxidized, in a pathway mitigating stomatal closure. Type II-GRXs might prevent oxidation of partners, the oxidized form of which could trigger closure. The roles of cytosolic NTRs and other TRs in guard cells remain to be determined.

Supporting information

Table S1. Leaf characteristics of 6 week-old plants and guard cell characteristics for evaluating the enrichment in guard cells in the broken and washed epidermal fraction.

Table S2: Proteins identified and quantified in guard cell-enriched and leaf fractions by mass spectrometry-based proteomics.

Table S3. List of cell wall and extracellular proteins identified in the guard cell-enriched fraction.

Table S4. List of proteins having transcript preferentially expressed in guard cell protoplasts (Leonhard et al., 2004) identified in the guard cell-enriched fraction.

Table S5. List of 14-3-3 proteins identified in the guard cell-enriched fraction.

Table S6. List of references cited in Table 1.

Figure S1: Transcriptomic analysis of *TR* expression in guard and mesophyll cell protoplasts. Data were retrieved from the microarray analyses described by Yang et al., (2008). RNA was isolated from protoplasts prepared from guard or mesophyll cells and hybridized to the ATH1 GeneChip. Two independent hybridization experiments per cell type were performed. Means and SD of expression levels

were retrieved using the Arabidopsis eFP Browser at bar-utoronto.ca (Winter et al., 2007). **A**, NADPH-Thioredoxin reductase A (NTRA) and thioredoxins h2, h3, h4, h5, h9, TDX, o1, o2, Clot, m3, Lillium-1 and CDSP32; **B**, Glutaredoxins S15 and ROXY10, peroxiredoxin II-B (II-B), glutathione peroxidase 2 (GPX2), and methionine sulfoxide reductases A1 and A4.

Figure S2. Gene expression in guard cells. *TRXh2* (**A**), *TRXh3* (**B**), *NTRB* (**C**) and *PRX-IIB* (**D**) gene promoters were fused to β-glucuronidase (*GUS*) as a reporter gene and gene expression was monitored in 15 day-old plants by histochemical analysis. Inset: focus on one single stomata.

Figure S3. Characterization of mutants deficient in the expression of *PRXQ* and *TRXh3* genes. A. Genotyping of SAIL_742_G10 plants (*prxq)* using primers corresponding to 5' and 3' ends of *PRXQ* coding sequence. **B**. Genotyping of SAIL_314_G04 (*trxh3-1*) using primers corresponding to 5' and 3' ends of *TRXh3* coding sequence. WT: wild type. **C**. Western blot analysis of PRXQ abundance in WT and *prxq* plants. **D**. Western blot analysis of TRX h3 abundance in WT, *trxh3-1* (homozygous SAIL_742_G10) and *trxh3-2* (homozygous SALK_111160) plants.

Figure S4. Growth of plants modified for the expression of various *TR* genes. Plants were grown for 5 or 6 weeks in control conditions: moderate light (200 µmol photons.m^{-2}.s^{-1}) and short photoperiod (8 h) at 22°C. Rosette weight values are means ± SD of four to six average values originating from independent experiments (at least 6 plants for each genotype per experiment). * and ***, significantly different from the WT value with $P < 0.05$ and $P < 0.001$, respectively (*t*-test). *2cprx*, double *2cysprxa 2cysprxb* mutant plants (**A**); *ntra ntrb*, double *ntra ntrb* mutant plants (**B**); *prxq* (**A**), *grxs17* (**C**), *trxh3-1, trxh3-2* (**D**) and *trxo1-1, trxo1-2* (**E**) mutants lacking PRXQ, GRXS17, TRXh3 and TRXo1, respectively.

Figure S5. Photograph of wild type (WT) plants and of plants modified for the expression of various *TR* genes. Plants were grown for 5 weeks in control conditions: moderate light (200 µmol photons.m^{-2}.s^{-1}) and short photoperiod (8 h) at 22°C. *2cprx*, double *2cysprxa 2cysprxb* mutant plant; *ntra ntrb*, double *ntra ntrb* mutant plant; KI1 and KI2, independent *grxS14* GRXS16-RNAi lines.

Figure S6. Leaf chlorophyll content of plants modified for the expression of various *TR* genes. Plants grown for 6 weeks in control conditions: moderate light (200 µmol photons.m^{-2}.s^{-1}) and short photoperiod (8 h) at 22°C. Data are means ± SD of at least 5 values originating from adult leaves from independent plants. ***, significantly different from the WT value with $P < 0.001$, (*t*-test). *2cprx*, double *2cysprxa 2cysprxb* mutant plants; *ntra ntrb*, double *ntra ntrb* mutant plants; *prxq, grxs17*, *trxh3* and *trxo1*, mutants lacking PRXQ, GRXS17, TRXh3 and TRXo1, respectively.

Figure S7. Stomatal density (A and C) and stomatal index (B and D) of Arabidopsis lines affected in the expression of genes coding for various types of thiol reductases. Data are means ± SD of 12 independent values using peeled epidermis from three leaves per genotype. Plants were grown for 4 weeks in control conditions: moderate light (200 µmol photons.m^{-2}.s^{-1}) and short photoperiod (8 h) at 22°C. *grxs17*, *trxh3*, *trxo1* and *grxs14*, mutants lacking GRXS17, TRXh3, TRXo1 and GRXS14, respectively; C-GRXS16 C2 and C4, two independent *GRXS16*-cosuppressed lines; OE-GRXS16 O4 and O5, two independent *GRXS16*-overexpressing lines.

Figure S8. Stomatal conductance of Arabidopsis lines affected in the expression of genes coding for various types of thiol reductases. Measurements of the water efflux from leaf abaxial side were performed using porometry on plants grown for 6 weeks in control conditions. Conductance values are means ± SD of six average values originating from independent plants (8 measurements per plant for each genotype per experiment); *trxh3* (**A**-**B**), *trxo1* (**C**) and *grxs17* (**D**), mutants lacking TRXh3, TRXo1 and GRXS17, respectively; *grxs14* and OE-GRXS14 OE1 (**E**), lines lacking *GRXS14* expression and overexpressing *GRXS14*, respectively; C-GRXS16 C2 and C4 (**F**), two independent *GRXS16*-cosuppressed lines; OE-GRXS16 O4 and O5 (**G**), two independent *GRXS16*-overexpressing lines.

Summary statement: The contribution of thiol reductases to the signaling network governing stomatal functioning remains poorly known. Using proteomics, we show that numerous thiol reductases are abundant in a guard cell-enriched fraction, and we unveil a stomatal phenotype in Arabidopsis mutants for thiol reductases.

Figure 1

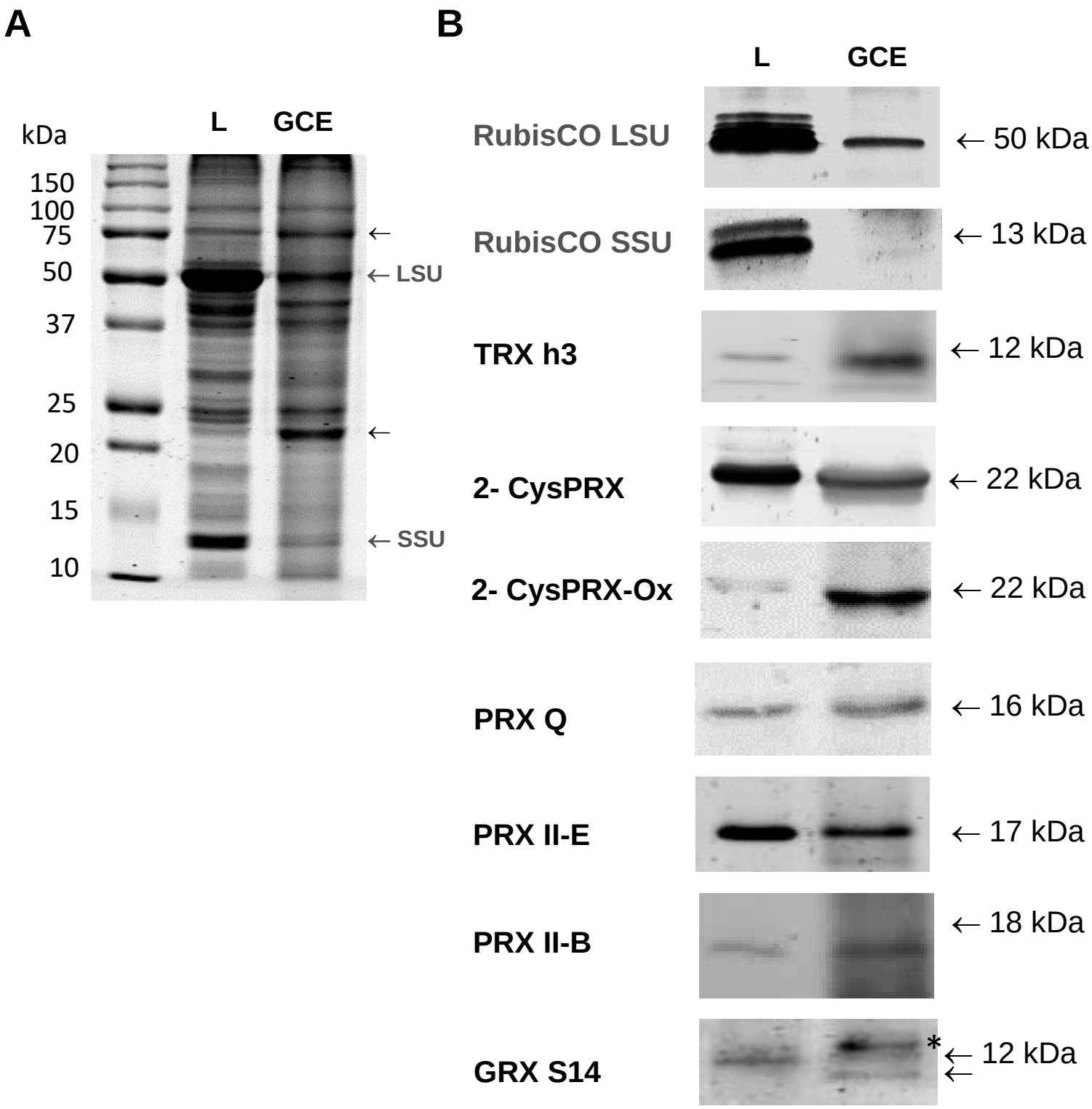

Figure 1 Western blot analysis of the abundance of thiol reductases in extracts from a guard cell-enriched fraction **A.** Coomassie Blue-stained gel of SDS-PAGE separated proteins from leaf blades (L) and GCE fractions. The arrows indicate proteins more abundant in the GCE fraction. LSU and SSU, large and small RubisCO subunits, respectively. **B.** Western blot analysis of RubisCO subunits and of various types of thiol reductases in L and GCE fractions. Blots (20 to 30 µg proteins per lane, depending on the serum used, for both fractions) were probed using antibodies raised against RubisCO (1:10,000), TRX h3 (1:20,000), 2-CysPRX (1:10,000) 2-CysPRX-Ox, hyperoxidized 2-CysPRX (1:4000), PRXQ (1:1000), PRX-IIE (1:10,000) PRXII-B (1:20,000) and GRXS14 (1:800). For the latter, the asterisk points to a non-specific band and the two arrows indicate two GRX redox forms.

Figure 2

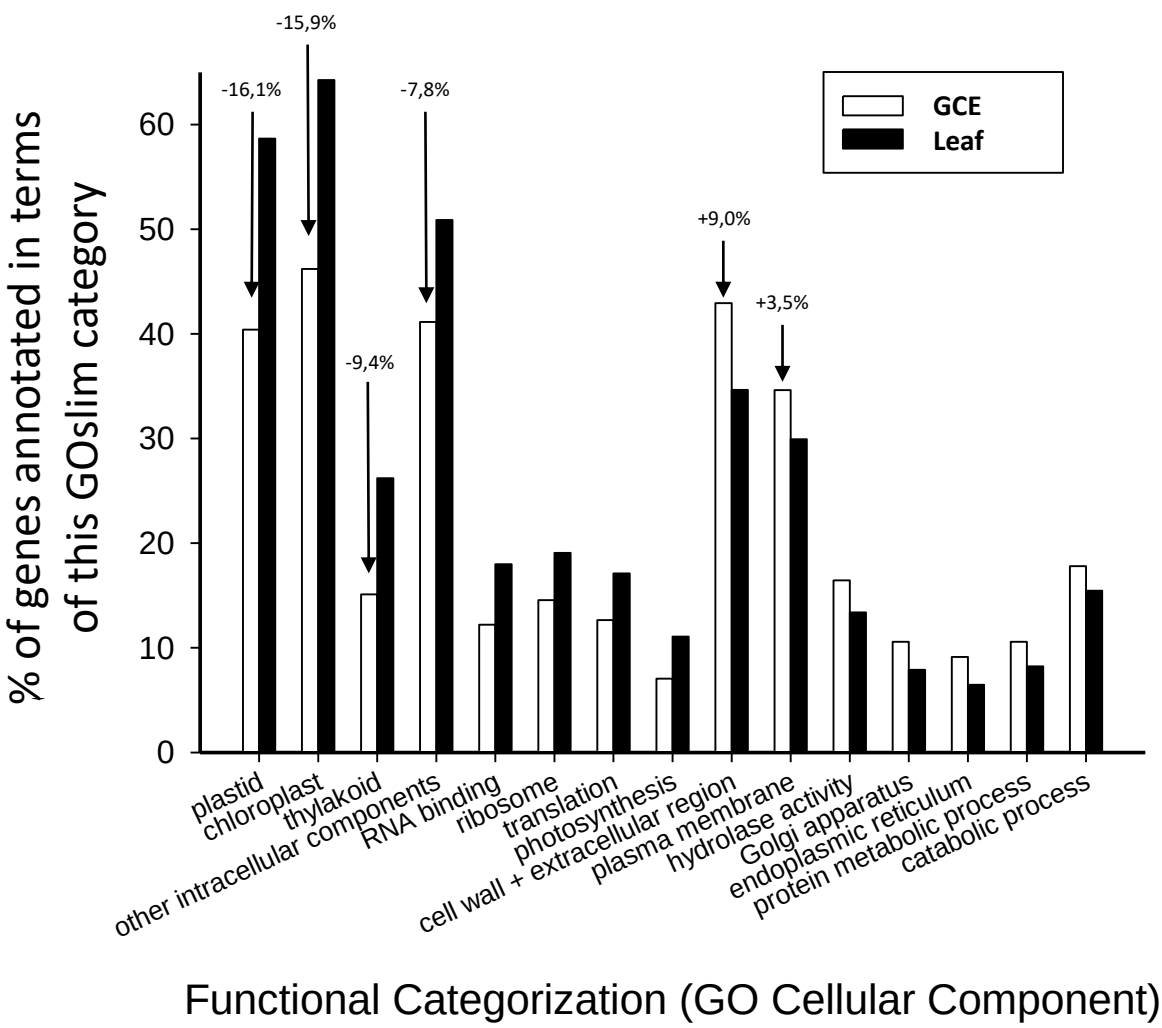

Figure 2: Functional categorization was performed by making use of the GO annotation retrieval tool available on the site TAIR: https://www.arabidopsis.org/tools/bulk/go/index.jsp. Analysis was retrieved on genes encoding the 25% most abundant proteins of each sample (in broken epidermis, 1174 proteins having a Log_2 of imputed normiBAQ ≥ 23,93 and in leaf, 1063 proteins ≥ 23.66)

Figure 3

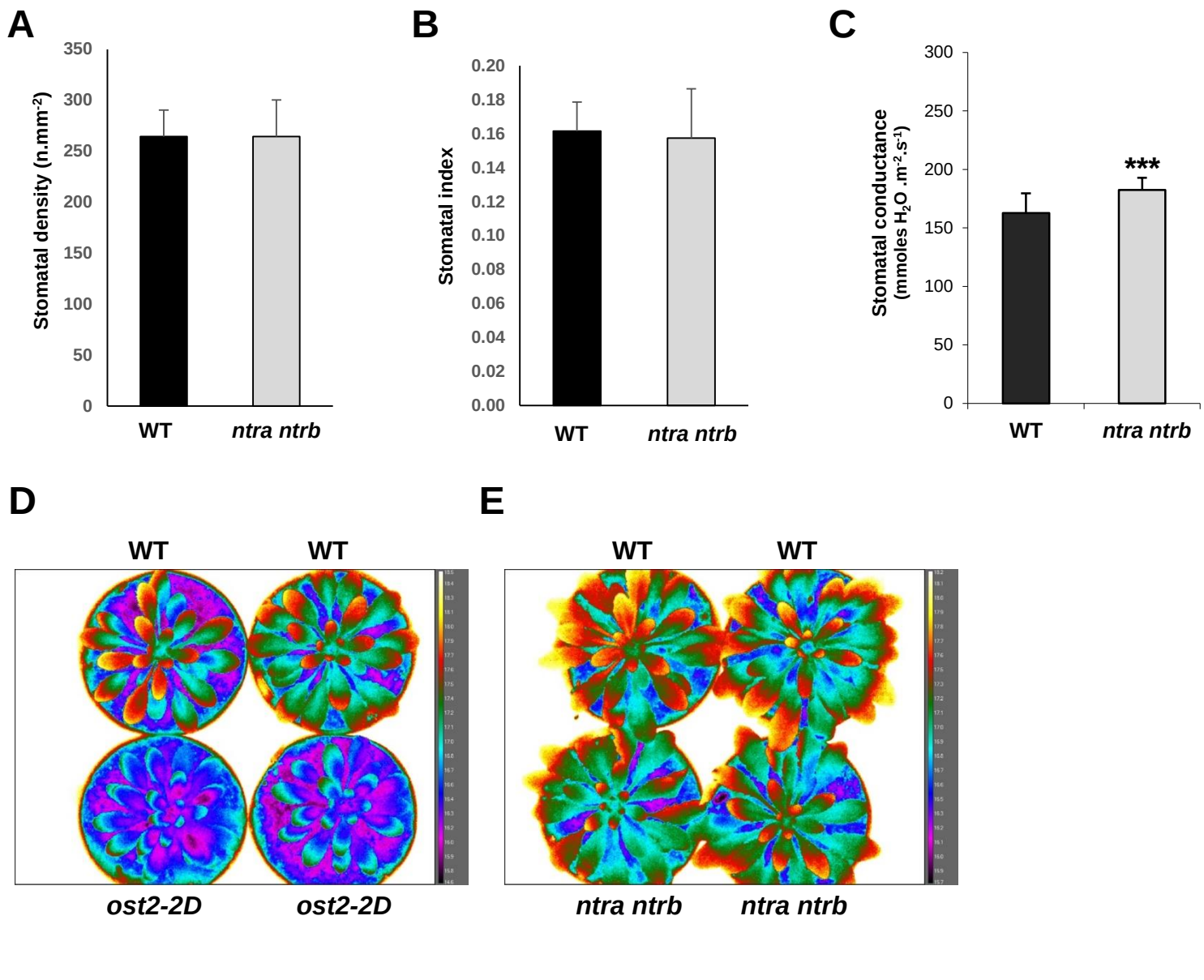

Figure 3. Stomatal phenotype of the Arabidopsis *ntra ntrb* mutant

A. Stomatal density. **B**. Stomatal index. Data for **A** and **B** are means ± SD of 12 independent values using peeled epidermis from three leaves per genotype. Plants were grown for 4 weeks in control conditions: moderate light (200 µmol photons.m^{-2}.s^{-1}) and short photoperiod (8 h) at 22°C. **C.** Stomatal conductance measurements using porometry. Measurements of the water efflux from leaf abaxial side were performed on plants grown for 6 weeks in control conditions. Conductance values are means ± SD of twelve average values per genotype originating from independent plants (8 measurements per plant for each genotype per experiment). ***, significantly different from the WT value with $P < 0.001$ (*t*-test). **D**. and **E**. Infrared thermal imaging. Plants were dark-adapted. False colored infrared images of 6-week-old plants grown in control conditions. The color scale on the right shows increasing temperature from purple to yellow. Pictures were taken at the end of the night period two hours before the light period. As a control, the *ost2-2D* mutant was used and shown to exhibit lower leaf temperature due to open stomata in the dark (Merlot et al., 2007). *ntra ntrb*, double *ntra ntrb* mutant plants.

Figure 4

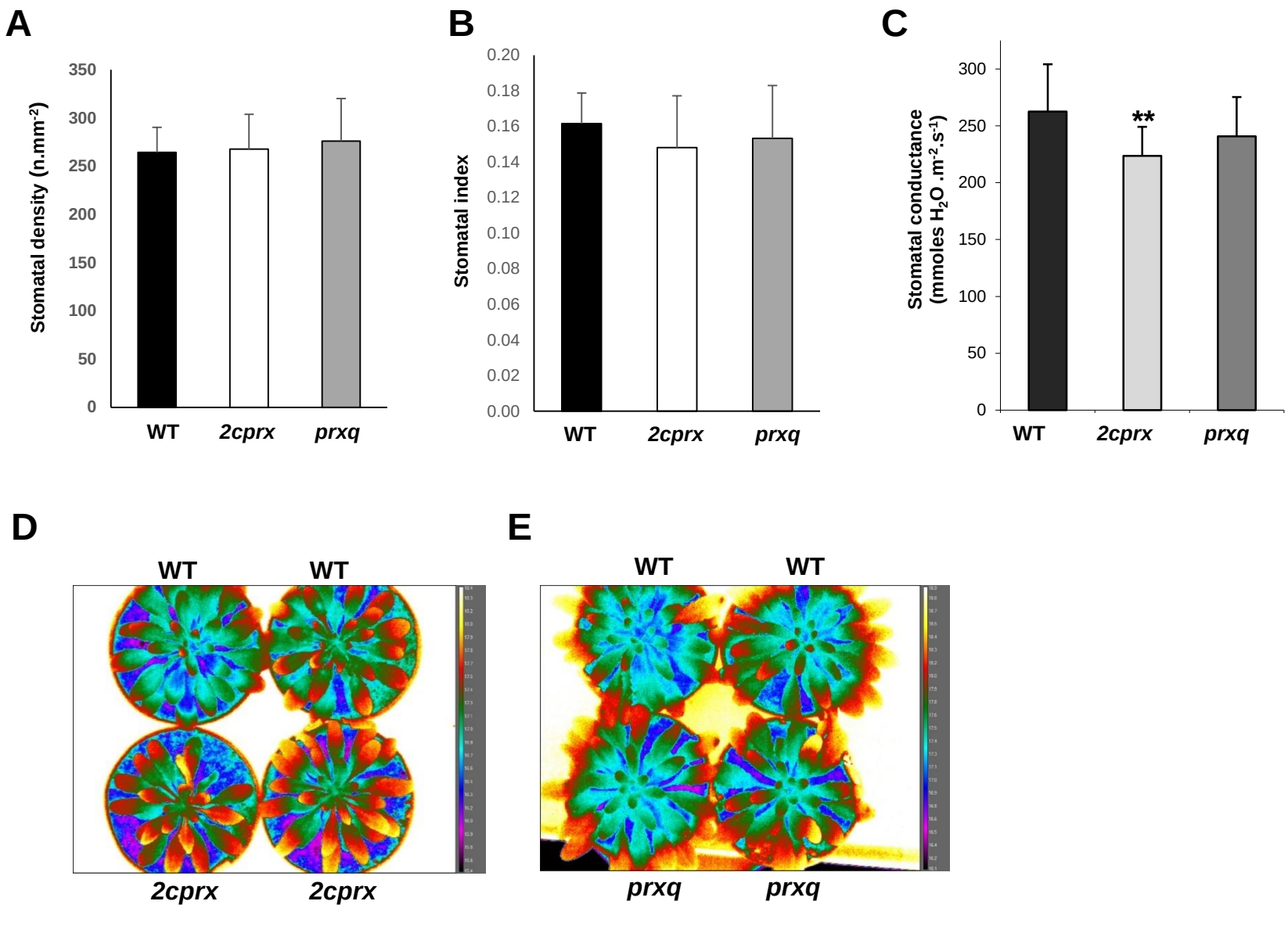

Figure 4. Stomatal phenotype of Arabidopsis mutants deficient in plastidial PRXs

A. Stomatal density. **B**. Stomatal index. Data for **A** and **B** are means ± SD of 12 independent values using peeled epidermis from three leaves per genotype. Plants were grown for 4 weeks in control conditions: moderate light (200 µmol photons.m^{-2}.s^{-1}) and short photoperiod (8 h) at 22°C. **C.** Stomatal conductance measurements using porometry. Measurements of the water efflux from leaf abaxial side were performed on plants grown for 6 weeks in control conditions. Conductance values are means ± SD of eight average values per genotype originating from independent plants (8 measurements per plant for each genotype per experiment). **, significantly different from the WT value with $P < 0.01$ (*t*-test). **D**. and **E.** Infrared thermal imaging. Plants were dark-adapted. False colored infrared images of 6-week-old plants grown in control conditions. The color scale on the right shows increasing temperature from purple to yellow. Pictures were taken at the end of the night period two hours before the light period. *2cprx*, double *2cysprxa 2cysprxb* mutant plants; *prxq*, knockout *PRXQ* plants.

Figure 5

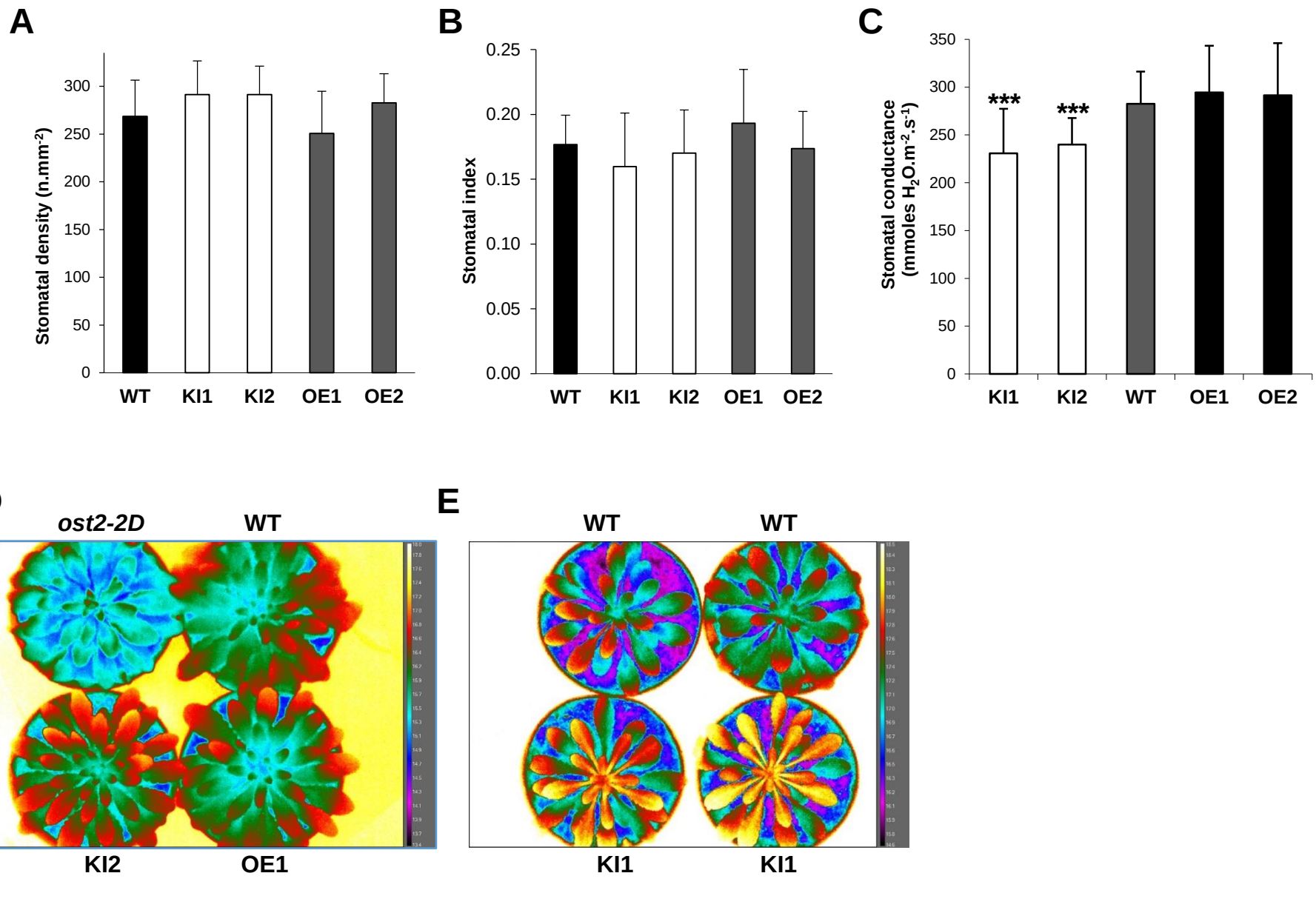

Figure 5. Stomatal phenotype of Arabidopsis lines modified for plastidial type-II GRXs. A. Stomatal density. **B**. Stomatal index. Data for **A** and **B** are means ± SD of 12 independent values using peeled epidermis from three leaves per genotype. Plants were grown for 4 weeks in control conditions: moderate light (200 µmol photons.m^{-2}.s^{-1}) and short photoperiod (8 h) at 22°C. **C.** Stomatal conductance measurements using porometry. Measurements of the water efflux from leaf abaxial side were performed on plants grown for 6 weeks in control conditions. Conductance values are means ± SD of at least 17 average values per genotype originating from independent plants (8 measurements per plant for each genotype per experiment). ***, significantly different from the WT value with $P < 0.001$ (*t*-test). **D**. and **E**. Infrared thermal imaging. Plants were dark-adapted. False colored infrared images of 6-week-old plants grown in control conditions. Pictures were taken at the end of the night period two hours before the light period. The color scale on the right shows increasing temperature from purple to yellow. As a control, the *ost2-2D* mutant was used and shown to exhibit lower leaf temperature due to open stomata in the dark (Merlot et al., 2007). KI1 and KI2, independent *grxS14* GRXS16-RNAi lines; OE1 and OE2, independent *GRXS14*-overexpressing lines.

Figure 6

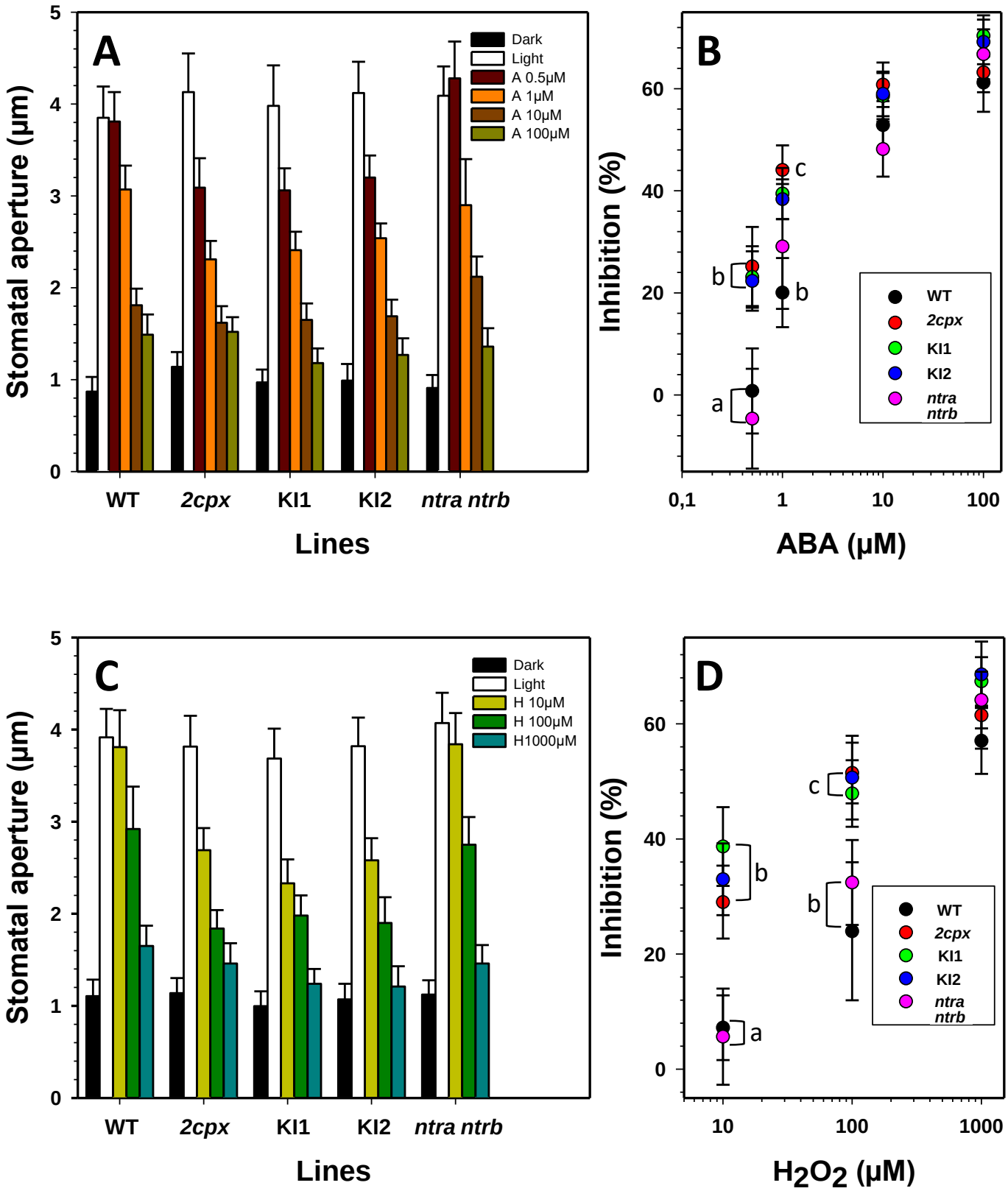

Figure 6. Effect of ABA and H_2O_2 on stomatal aperture in Arabidopsis mutants deficient in cytosolic NTRs, plastidial 2Cys-PRXs or plastidial type-II GRXs.

Stomatal aperture measurements in response to ABA concentrations of 0.5, 1, 10 and 100 µM (**A-B**) or to H_2O_2 concentrations of 10, 100 and 1000 µM (**C-D**) in light-treated epidermis. Data in panels **B** and **D** were calculated from the original raw data reported in panels **A** and **C**, respectively, and represent the inhibitions of stomatal aperture due to the treatments expressed in percents of that measured in light alone. Data represent means ± SD of 2 independent experiments with 60 measurements per genotype and treatment. Means were compared with the ANOVA test, and letters represent groups of means not statistically different ($P<0.05$). *2cprx*, double *2cysprxa 2cysprxb* mutant plants; KI1 and KI2, independent *grxS14* GRXS16-RNAi lines; *ntra ntrb*, double *ntra ntrb* mutant plants.

Figure 7

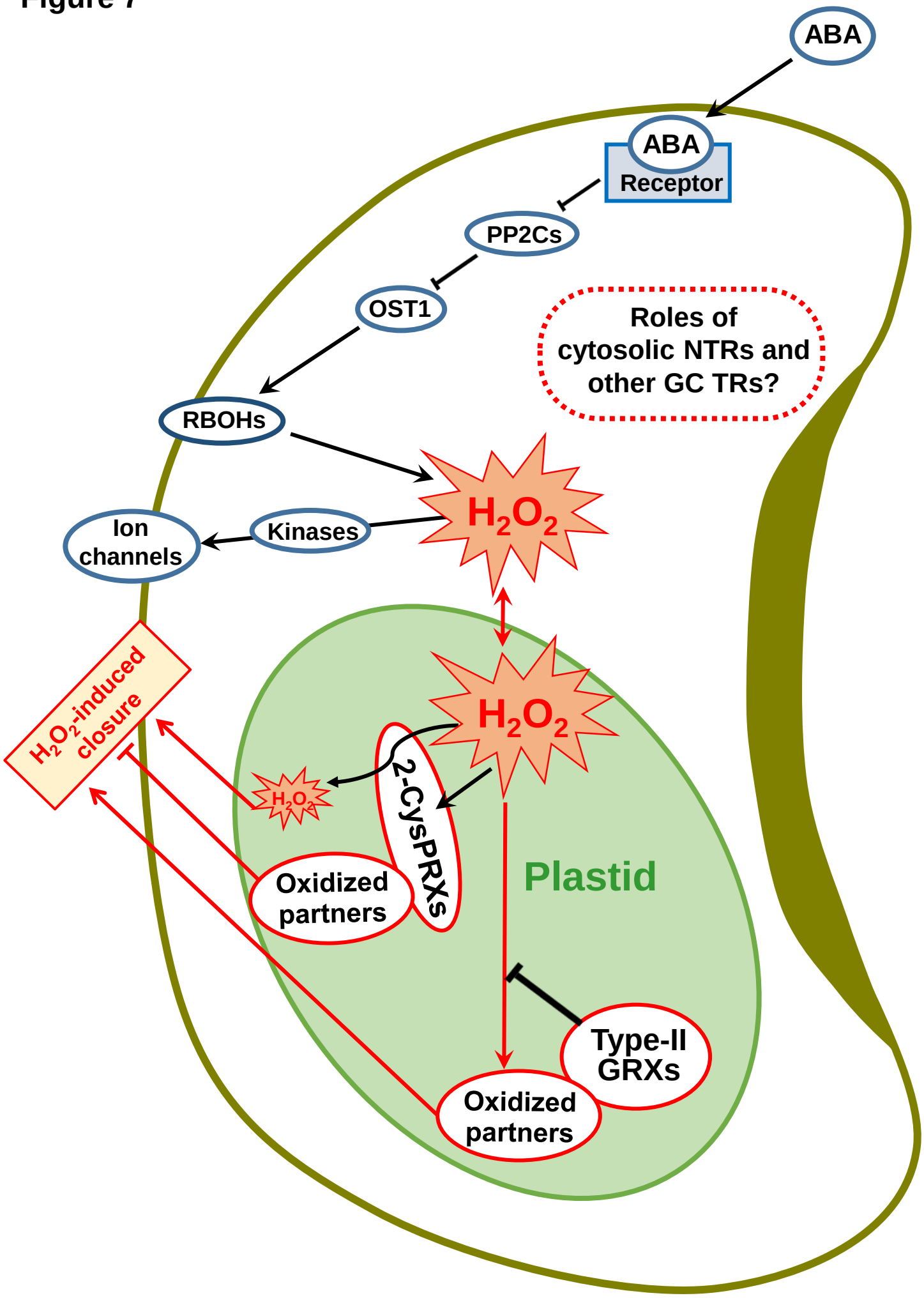

Figure 7. Model for positioning putative roles of plastidial 2-CysPRXs and type-II GRXs in the signaling network governing stomatal closure. Based on the results gained on epidermal peels showing modified responses of mutants to ABA and H_2O_2 and the known biochemical functions of these enzymes, we propose that they participate in H_2O_2-related transduction pathways. 2-CysPRXs might scavenge H_2O_2 within plastid or promote oxidation of partners that remain to be identified and are involved, when oxidized, in a pathway mitigating stomatal closure. Type II-GRXs might prevent oxidation of partners, the oxidized form of which could trigger closure. The roles of cytosolic NTRs and other TRs in guard cells remain to be determined.

Figure S1

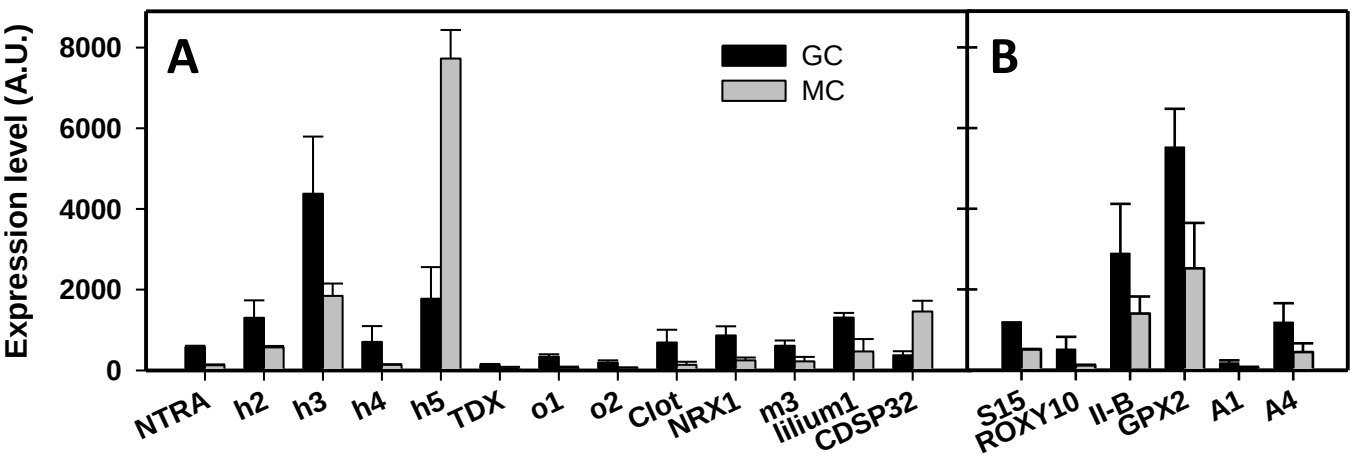

Figure S1: Transcriptomic analysis of *TR* expression in guard and mesophyll cell protoplasts. Data were retrieved from the microarray analyses described by Yang et al., (2008). RNA was isolated from protoplasts prepared from guard or mesophyll cells and hybridized to the ATH1 GeneChip. Two independent hybridization experiments per cell type were performed. Means and SD of expression levels were retrieved using the Arabidopsis eFP Browser at bar-utoronto.ca (Winter et al., 2007). Only *TR* genes displaying GC/MC or MC/GC ratios of expression ≥ 2 were considered for this figure. **A**, NADPH-Thioredoxin reductase A (NTRA) and thioredoxins h2, h3, h4, h5, TDX, o1, o2, Clot, m3, Lillium-1 and CDSP32; **B**, Glutaredoxins S15 and ROXY10, peroxiredoxin II-B (II-B), glutathione peroxidase 2 (GPX2), and methionine sulfoxide reductases A1 and A4.

Figure S2

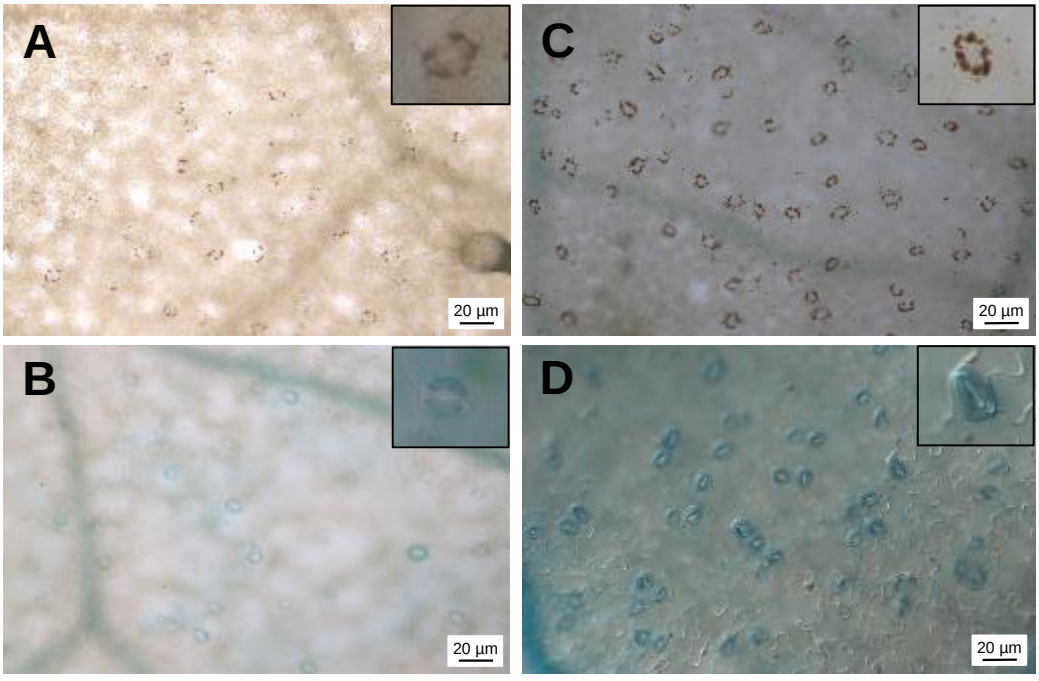

Figure S2. Gene expression in guard cells. *TRXh2* (A), *TRXh3* (B), *NTRB* (C) and *PRX-IIB* (D) gene promoters were fused to β-glucuronidase (*GUS*) as a reporter gene and gene expression was monitored in 15 day-old plants by histochemical analysis. Inset: focus on one single stomata.

Figure S3

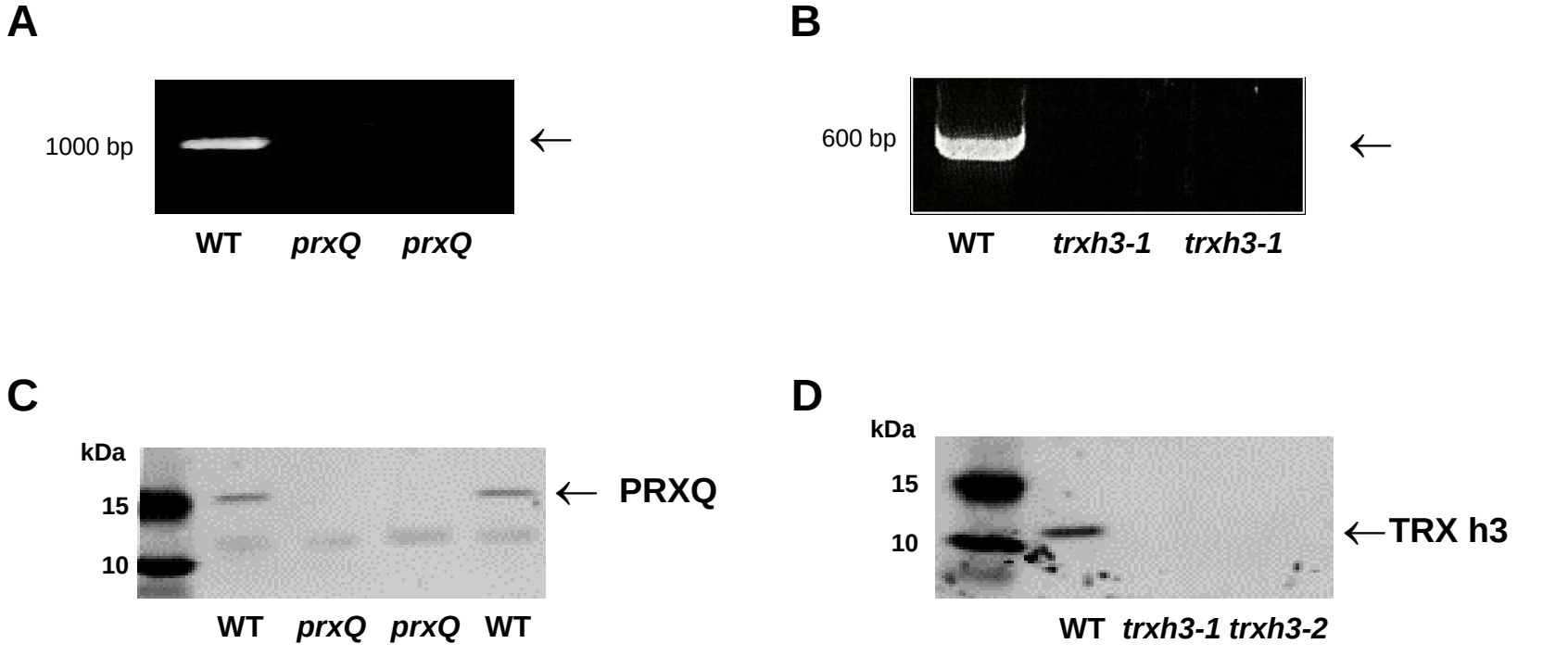

Figure S3. Characterization of mutants deficient in the expression of *PRXQ* and *TRXh3* genes.

A. Genotyping of SAIL_742_G10 plants (*prxq)* using primers corresponding to 5' and 3' ends of *PRXQ* coding sequence. **B**. Genotyping of SAIL_314_G04 (*trxh3-1*) using primers corresponding to 5' and 3' ends of *TRXh3* coding sequence. WT: wild type. **C**. Western blot analysis of PRXQ abundance in WT and *prxq* plants. **D**. Western blot analysis of TRX h3 abundance in WT, *trxh3-1* (homozygous SAIL_742_G10) and *trxh3-2* (homozygous SALK_111160) plants.

Figure S4

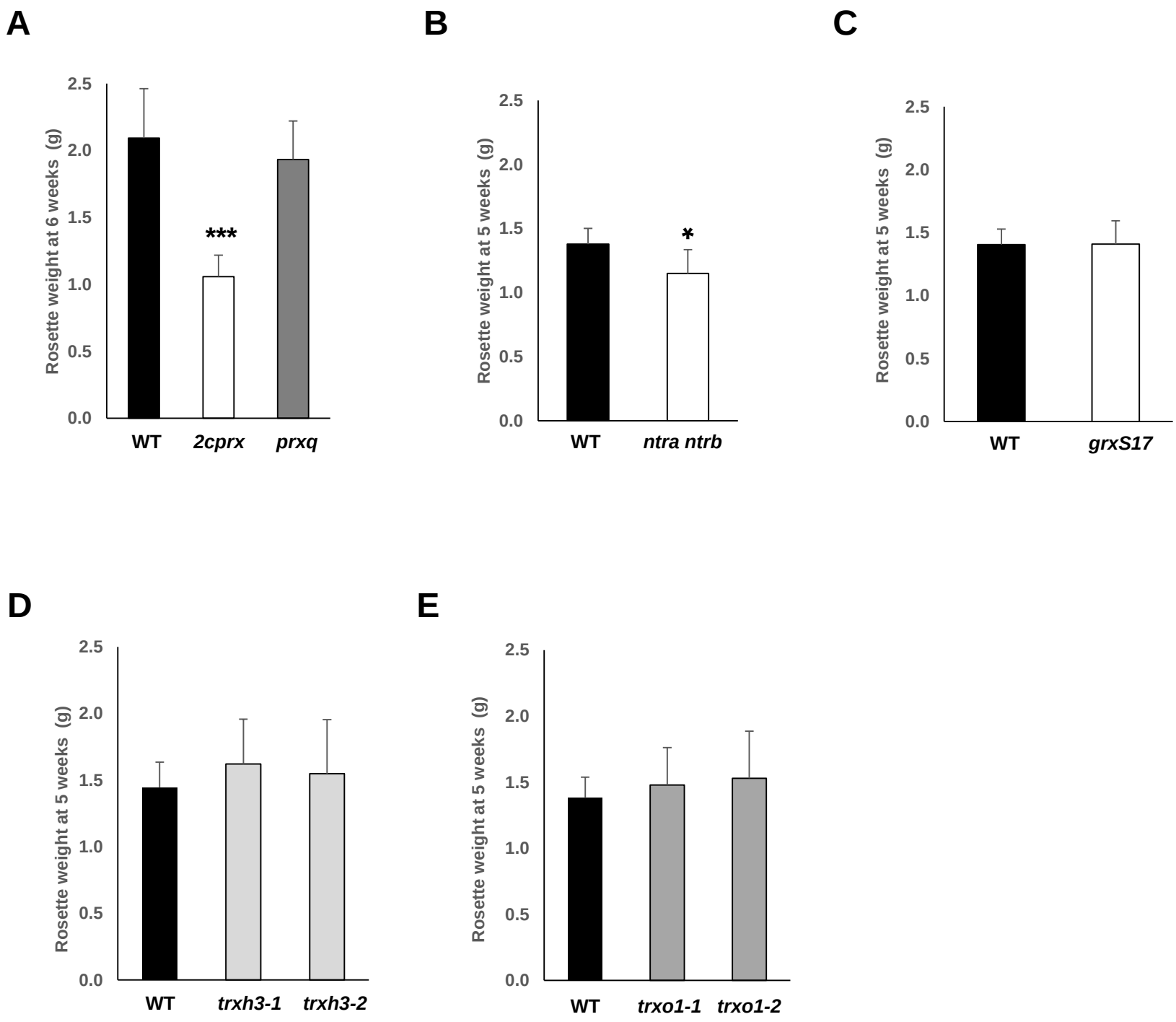

Figure S4. Growth of plants modified for the expression of various *TR* genes. Plants were grown for 5 or 6 weeks in control conditions: moderate light (200 µmol photons.m^{-2}.s^{-1}) and short photoperiod (8 h) at 22°C. Rosette weight values are means ± SD of four to six average values originating from independent experiments (at least 6 plants for each genotype per experiment). * and ***, significantly different from the WT value with $P < 0.05$ and $P < 0.001$, respectively (*t*-test). *2cprx*, double *2cysprxa 2cysprxb* mutant plants (**A**); *ntra ntrb*, double *ntra ntrb* mutant plants (**B**); *prxq* (**A**), *grxs17* (**C**), *trxh3-1, trxh3-2* (**D**) and *trxo1-1, trxo1-2* (**E**) mutants lacking PRXQ, GRXS17, TRXh3 and TRXo1, respectively.

Figure S5

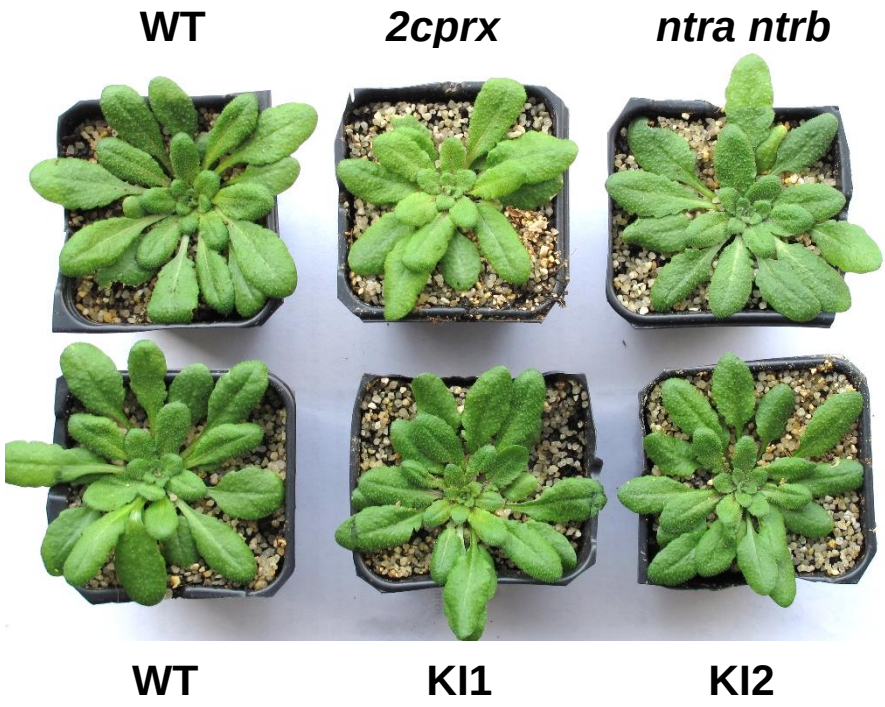

Figure S5. Photograph of wild type (WT) plants and of plants modified for the expression of various *TR* genes. Plants were grown for 5 weeks in control conditions: moderate light (200 µmol photons.m^{-2}.s^{-1}) and short photoperiod (8 h) at 22°C. *2cprx*, double *2cysprxa 2cysprxb* mutant plant ; *ntra ntrb*, double *ntra ntrb* mutant plant; KI1 and KI2, independent *grxS14* GRXS16-RNAi lines..

Figure S6

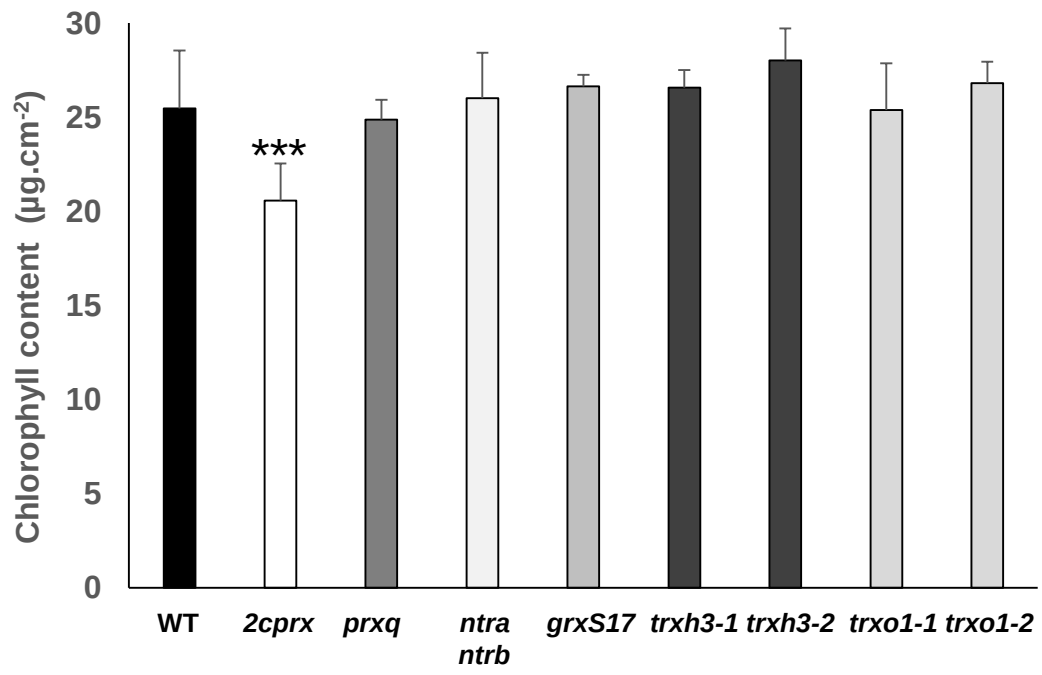

Figure S6. Leaf chlorophyll content of plants modified for the expression of various *TR* genes.
Plants grown for 6 weeks in control conditions: moderate light (200 µmol photons.m^{-2}.s^{-1}) and short photoperiod (8 h) at 22°C. Data are means ± SD of at least 5 values originating from adult leaves taken from independent plants. ***, significantly different from the WT value with $P < 0.001$, (*t*-test). *2cprx*, double *2cysprxa 2cysprxb* mutant plants; *ntra ntrb*, double *ntra ntrb* mutant plants; *prxq*, *grxs17*, *trxh3* and *trxo1*, mutants lacking PRXQ, GRXS17, TRXh3 and TRXo1, respectively.

Figure S7

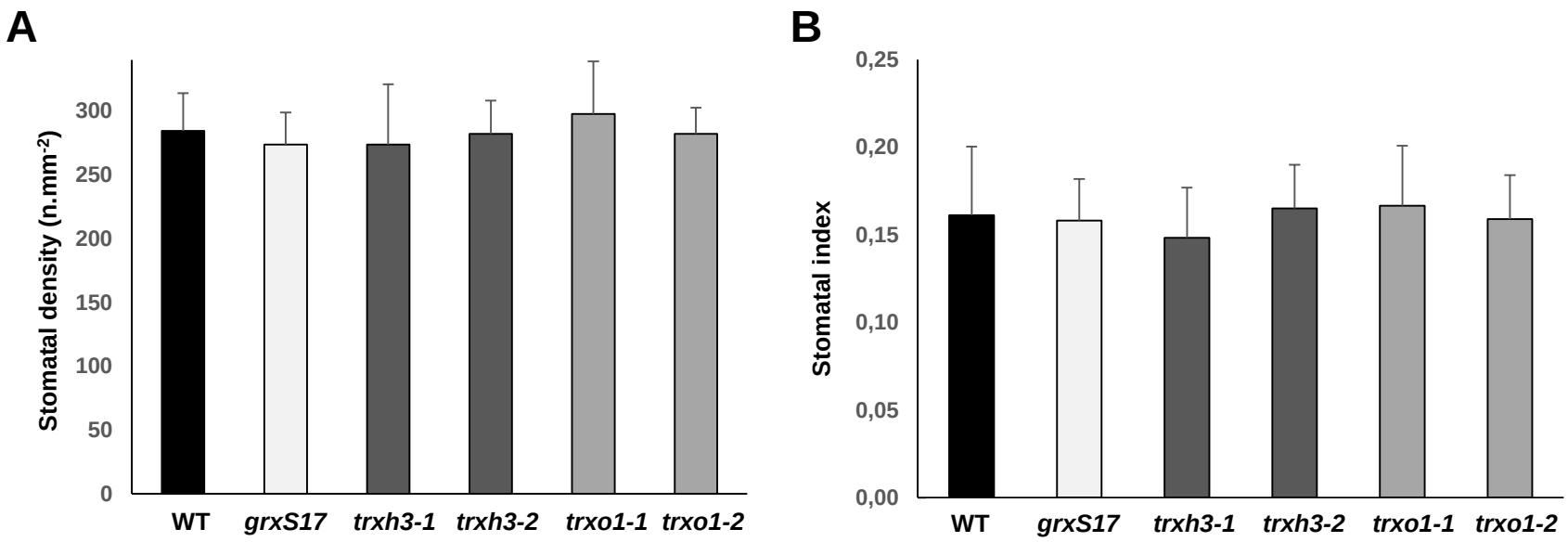

Figure S7. Stomatal density (A and C) and stomatal index (B and D) of Arabidopsis lines affected in the expression of genes coding for various types of thiol reductases. Data are means ± SD of 12 independent values using peeled epidermis from three leaves per genotype. Plants were grown for 4 weeks in control conditions: moderate light (200 µmol photons.m^{-2}.s^{-1}) and short photoperiod (8 h) at 22°C. *grxs17*, *trxh3*, *trxo1* and *grxs14*, mutants lacking GRXS17, TRXh3, TRXo1 and GRXS14, respectively; C-GRXS16 C2 and C4, two independent *GRXS16*-cosuppressed lines; OE-GRXS16 O4 and O5, two independent *GRXS16*-overexpressing lines.

Figure S8

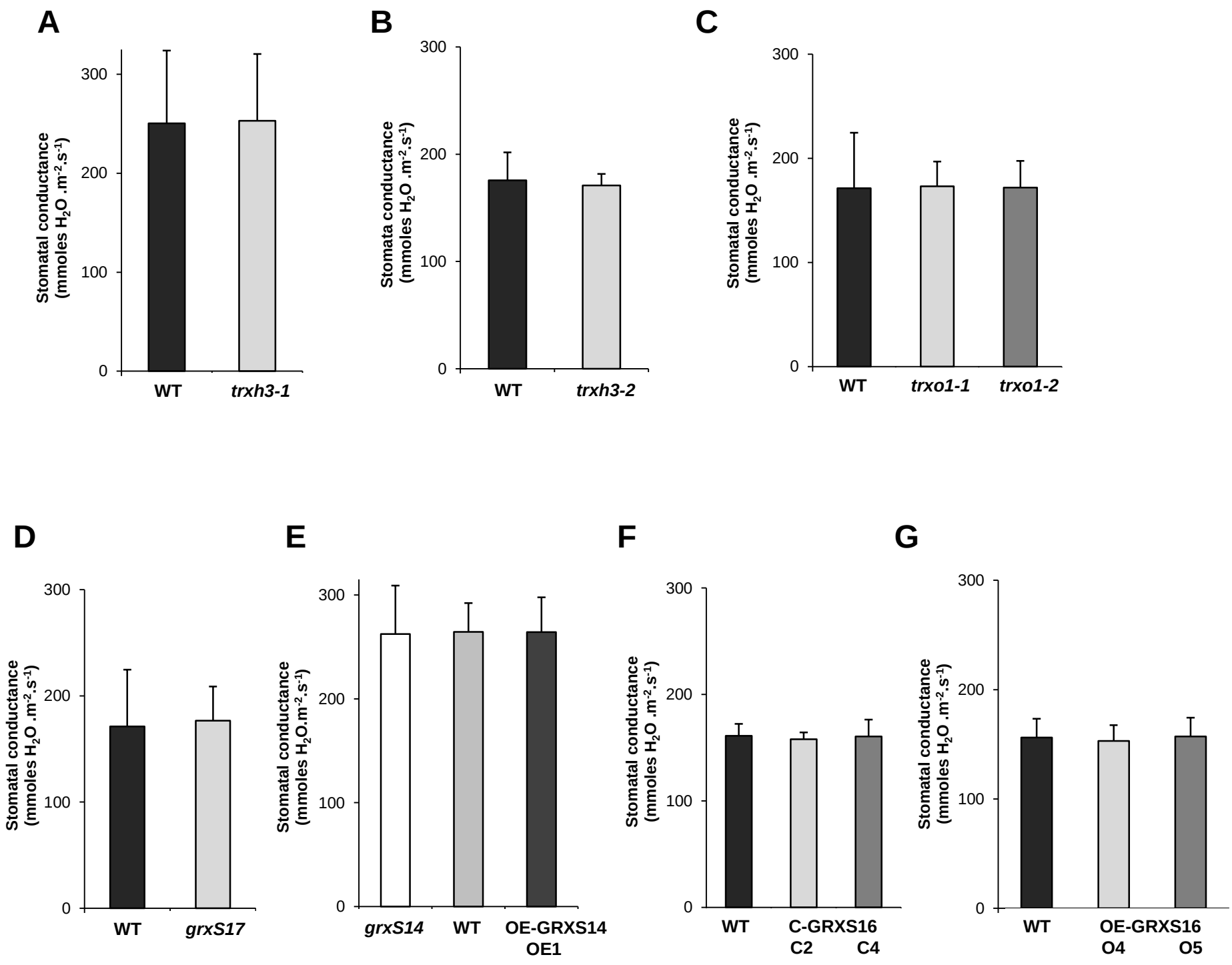

Figure S8. Stomatal conductance of Arabidopsis lines affected in the expression of genes coding for various types of thiol reductases. Measurements of the water efflux from the leaf abaxial side were performed using porometry on plants grown for 6 weeks in control conditions. Conductance values are means ± SD of six average values originating from independent plants (8 measurements per plant for each genotype per experiment); *trxh3* (**A**-**B**), *trxo1* (**C**) and *grxs17* (**D**), mutants lacking TRXh3, TRXo1 and GRXS17, respectively; *grxs14* and OE-GRXS14 OE1 (**E**), lines lacking *GRXS14* expression and overexpressing *GRXS14*, respectively; C-GRXS16 C2 and C4 (**F**), two independent *GRXS16*-cosuppressed lines; OE-GRXS16 O4 and O5 (**G**), two independent *GRXS16*-overexpressing lines.